Sustainable Structures
ISSN: 2789-3111 (Print); ISSN: 2789-312X (Online)
http://www.sustain-dpl.com/journal/sust
DOI: 10.54113/j.sust.2024.000060

ORIGINAL ARTICLE

Behaviour of post-tensioned benches made of high-content recycled aggregate concrete reinforced with racquet string fibres

Narakorn Suwannachote [a], Thanongsak Imjai [b,*], Fetih Kefyalew [b], Radhika Sridhar [b], Reyes Garcia [c], U. Johnson Alengaram [d], Sivakumar Naganathan [e]

[a] School of Languages and General Education, Walailak University, Nakhon Si Thammarat 80161, Thailand
[b] School of Engineering and Technology, Walailak University, Nakhonsithammarat 80161, Thailand
[c] Civil Engineering Stream, School of Engineering, The University of Warwick, Coventry, CV4 7AL, UK
[d] Centre for Innovative Construction Technology (CICT), Department of Civil Engineering, Faculty of Engineering, Universiti Malaya, 50603, Kuala Lumpur, Malaysia
[e] School of Engineering, Sri Sivasubramaniya Nadar (SSN) College of Engineering, Chennai, Tamil Nadu 600020, India
***** *Correspondence: thanongsak.im@wu.ac.th; Tel.: +66 (0) 7567 2378*

Abstract: This study investigates the serviceability and structural behaviour of a new type of recycled aggregate concrete (RAC) bench with waste badminton racquet fibres. Twenty-one cantilever benches were tested in two Series with different fibre volume fractions (V_f = 0%, 0.5%, 1.0% or 1.5%). The RAC had 100% of natural aggregates replaced with recycled concrete aggregate (RCA). The benches in Series II were post-tensioned in flexure using an innovative Post-Tensioned Metal Strapping (PTMS) technique using 1, 2 or 3 straps. Tests were carried out to evaluate 1) static loading behaviour, 2) long-term behaviour after 365 days of sustained loading, and 3) human-induced vibrations. The static test results show that benches with 100% RAC and PTMS had higher capacity (by about 25%) that counterpart benches without PTMS. Hence, the maximum flexural strength of the cantilever bench was improved by 5.7% for the cantilever bench with PTMS strengthening, which further enhanced the flexural behaviour compared to the bench with only 1.5% of fibres. The human-induced vibration test results confirmed that the maximum vibration of the benches met the code limits for floor buildings. Finite element analyses of the RAC benches with PTMS were carried out in Abaqus®, and the experimental deflections agreed well (errors <5%) with the FEM results. A simplified fatigue life analysis confirmed that the RAC benches with PTMS can have a potential service life of up to 20 years. The use of glow-in-the-dark (GID) features into the benches in Series II enhanced their night-time visibility and visual appeal by up to 8 h. This research contributes towards the development of new applications for RAC with waste badminton racquet fibres, which can offer more sustainable solutions for the construction of urban furniture.

Keywords: Recycled aggregate concrete; urban furniture; badminton racquet fibres; vibrations; fatigue life; glow in the dark

1 Introduction

The construction and demolition of old infrastructure use huge amounts of natural resources and produce large amounts of construction and demolition waste (C&DW), with an estimated 923 million tons of C&DW in 2016 [1, 2]. The use of C&DW in construction itself can improve resource efficiency and contribute to the adoption of circular economy principles [3]. Much of the C&DW consists of

Received: 24 June 2024; Received in revised form: 4 September 2024; Accepted: 8 October 2024

concrete which, if adequately recycled and post-processed, can serve as recycled concrete aggregate (RCA). The use of RCA in the production of new recycled aggregate concrete (RAC) was previously studied [4-6], but technical challenges often limit its applicability. For instance, RCA has high water absorption (especially the fine fraction) due to the adhered cement mortar. RCA also contains impurities and cracks induced during the recovery/recycling process [7-9], which in turn reduce the RAC's mechanical properties. Mix optimisation can overcome some of these limitations so that RAC with high RCA replacement ratios (up to 100%) can be used in structural and non-structural applications. However, the use of high cement contents or mineral additives is often necessary for RAC to be used in structural applications [10], which in turn can increase costs and CO_2 emissions [11]. As a result, alternative uses of RAC in other construction applications are currently being explored.

Past research has shown that RAC can be successfully used in the construction of urban furniture [12,13], which generally have low compressive strength requirements and allow for the use of RACs with high replacement volumes of natural aggregates (NA). In the last years, fast economic development and population growth in Southeast Asian cities have led to a large demand for urban furniture. In such regions, physical and visual elements are extensively used in streetscapes to improve the built environment. A predominant piece of furniture in streetscapes is the bench, which serves as a space for interaction and social cohesion. Past research has shown that benches are seen as one of the top desirable features in public spaces in Thailand. Moreover, Thailand and the wider Southeast Asian region produce thousands of tons of RCA per day [14]. However, despite its potential benefits, the use of RAC in urban furniture in the country has not been explored.

To save materials, reduce weight and provide aesthetic appeal, benches with thin cross sections are often preferred over bulky and heavy counterparts. Nonetheless, thin concrete elements are prone to crack easily and thus they need some internal reinforcement [15-16] which can be provided using internal fibres. Badminton is one of the most popular sports across Southeast Asia. Due to the high stresses experienced by the string racquets during badminton matches, many strings often break, after which they are simply discarded for recycling. Whilst limited data exists for Thailand, it is estimated that up to 6 t of racquet strings are discarded per year in the country. However, recent research by the authors found that badminton string fibres have similar properties to those of low modulus of elasticity fibres used as internal reinforcement in concrete [17]. Fibres with low modulus of elasticity have been used to produce fibre reinforced concrete with good micro-cracking resistance at low stress levels as those typically experienced in service conditions [18]. Nonetheless, the use of badminton racquet string fibres as internal reinforcement in RAC has not been examined in the literature. The incorporation of discarded badminton string fibres into concrete can reduce waste and potentially reduce cracking of concrete. Another option to control cracking in slender concrete elements is the use of post-tensioned reinforcement [19-21]. However, the effect of post-tensioning in the vibration of thin-walled elements is not yet well understood and contradicting views exist in the current literature. Recent research [22] also recognised that the post-tensioning of RAC can be an effective way of recovering some of the properties lost due to the use of high RCA contents of up to 100%, as observed in previous studies [23-26]. Additional options also include the use of other fibres in concrete [27-28].

Urban furniture is always exposed to vibrations produced by users. For instance, users practicing outdoor sports in Southeast Asia tend to use benches as an exercise equipment, often standing, stretching or even jumping on them [29]. The vibration response of urban furniture can be evaluated through a forcing function, which causes elements to vibrate at the excitation's frequency. Frequency analysis provides information about structural vibrations, even in real-time. Random vibrations are present in nature as users interact with urban elements [30]. Random vibrations also quantify the average vibration levels over time across the frequency spectrum, which can provide further insight into the expected behaviour of a piece of furniture as users interact with it.

This study investigates the service and structural behaviour of a new type of urban bench cast with 100% RAC and waste badminton racquet fibres. Twenty-one cantilever benches were tested in two Series with different volume fractions of racquet fibres (V_f=0%, 0.5%, 1.0% and 1.5%). Tests were carried out to evaluate 1) static loading behaviour, 2) long-term behaviour after 365 days of sustained loading, and 3) human-induced vibrations. The benches in Series II were post-tensioned in flexure using an innovative PTMS technique. The novelty of this research focuses on developing RAC with waste

badminton fibres for non-structural concrete applications, specifically urban furniture. This research contributes towards the development of new applications for RAC with waste badminton fibres, which can offer more sustainable solutions for the construction of urban furniture.

2 Experimental programme

2.1 Design of benches

The bench (**Fig. 1**) is designed as a thin cantilever structure supported on a concrete block base which served as foundation. A thin cantilever bench was chosen as this is a common piece of urban furniture in southern Thailand, as well as being a functional and aesthetically appealing addition to the urban streetscape. Two Series of cantilever benches were built and tested:

1. Series I: Benches made with 100% RAC reinforced with waste badminton string fibres. This Series aims to benchmark the performance of the bench without any flexural reinforcement.

2. Series II: Post-tensioned benches made from 100% RAC reinforced with waste badminton string fibres. An innovative PTMS technique [31] was used to reduce deflections and vibrations observed in Series I.

To enhance its aesthetics, a strip of glow-in-the-dark (GID) [32] material is incorporated onto one of the Series II bench's sides, thus enhancing night-time visibility and making it visually appealing after dusk, as shown in **Fig. 1**. **Appendix A** includes additional construction details of the bench.

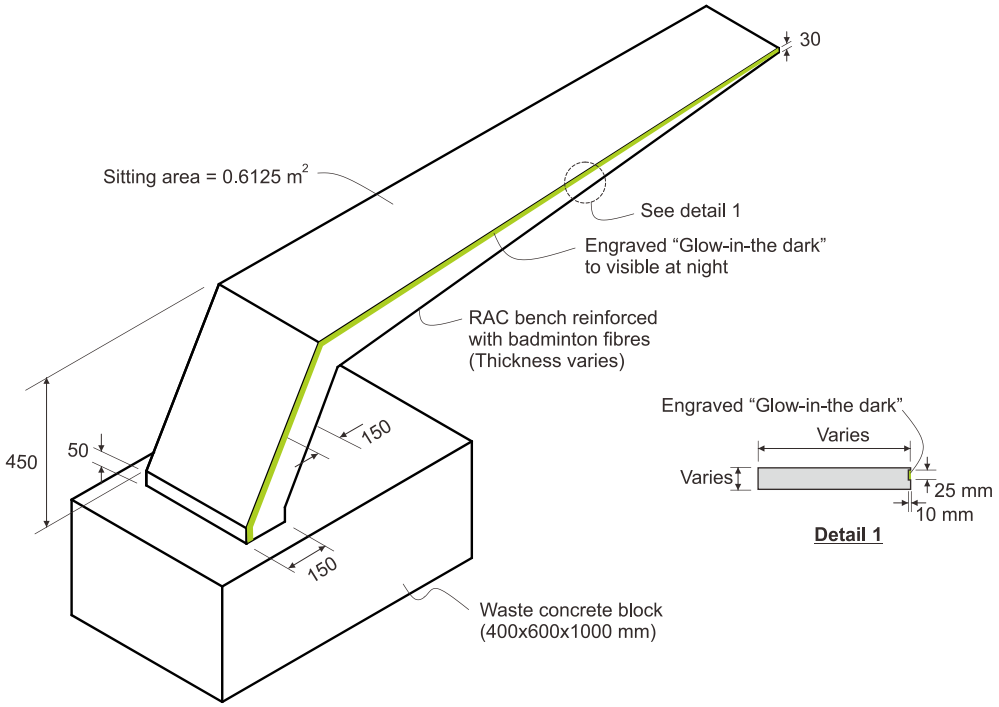

Fig. 1. General geometry of RAC bench (units: mm).

2.2 Materials

2.2.1 Recycled concrete aggregates

Both fine and coarse natural aggregate (NA) and RCA were used. The RCA was obtained from old concrete structures tested in the laboratory using a crushing machine. The original old concrete structures had a cylinder compressive strength of 45.0 MPa. The concrete crushed by the crushing machine was then sieved to obtain fine RCA of size 4.5 to 4.85 mm (RFA#1), and of size 2.3 to 2.5 mm (RFA#2). Likewise, coarse aggregate was obtained with size 9.5 to 10.5 mm (RCA#1), and size 19 to 20 mm (RCA#2), see **Fig. 2**. **Table 1** lists the properties of the NA and RCA used in this study. The specific gravity value and unit weight of RCA are approximately 10% and 19% lower than those of the NA, as shown in **Table 1**.

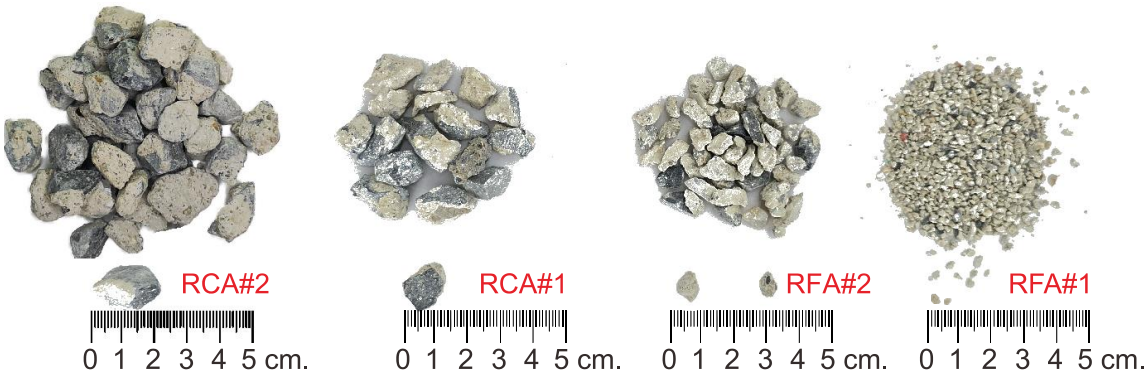

Fig. 2. Different sizes of RCA used to cast the benches.

Table 1. Physical and mechanical properties of NA and RCA

Properties	Coarse aggregates			Fine aggregates		
	Natural	RCA#2	RCA#1	Natural	RFA#2	RFA#1
Maximum size (mm)	20.2	19.5	10.3	4.81	4.68	2.36
Bulk specific gravity (SSD)	2.69	2.21	2.48	2.61	2.75	2.71
Unit weight (kg/m^3)	1745	1410	1436	1516	1395	1450
Water absorption (%)	0.29	4.23	5.21	1.12	2.61	2.79
Moisture (%)	0.63	2.16	2.21	1.43	2.43	2.56
Fineness modulus	-	-	-	2.68	1.83	1.90
Impact value (%)	10.23	13.40	12.45	-	-	-
Crushing value (%)	21.74	24.02	20.24	-	-	-
Residual mortar (%)	-	31.52	30.45	-	31.9	28.5

2.2.2 Waste badminton string fibres and internal reinforcement

Fig. 3 shows the typical waste racquet fibres used in the RAC, whereas **Table 2** summarises their physical and mechanical properties. The fibres were cut to size mechanically to ensure a consistent length (l_F) of 25 mm. The average modulus of elasticity (E_F) and tensile strength ($f_{t,F}$) of the fibres (one single fibre) were obtained by testing a total of 20 fibres according to ASTM D3379-75 [33]. The fibres were firmly gripped at both ends in a testing machine having a 1 kN capacity. The load on the single fibres was applied at 0.5 mm/min up to rupture of the fibre occurred.

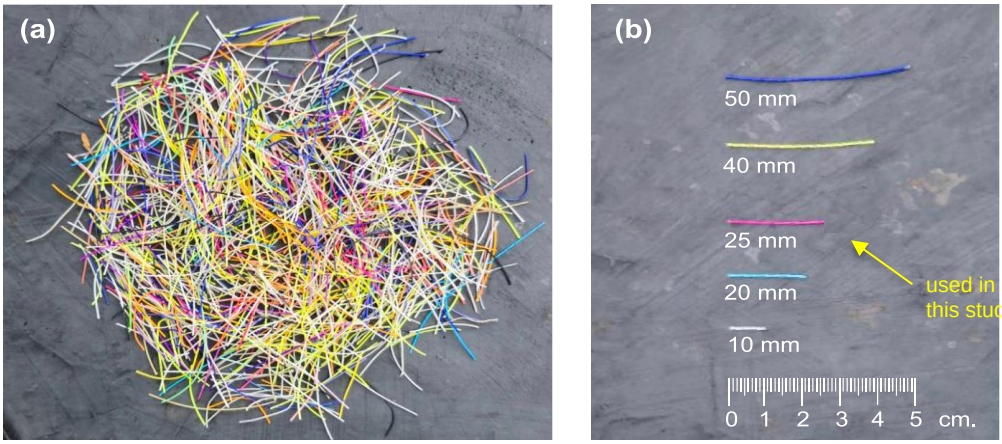

Fig. 3. (a) Waste badminton fibres, and (b) different fibre lengths obtained from cutting process and fibres.

Glass Fibre Reinforced Polymer (GFRP) reinforcement. Four GFRP bars of 12 mm diameter were used as dowel bars to anchor the bench to the concrete base. GFRP bars were used as single stirrups at a spacing of 83 mm, which were placed at the bench skeleton. Three GFRP stirrups (at a spacing of 50 mm) were also placed at the bench-concrete base, under the level of the infill soil. All the GFRP stirrups had a diameter of 9 mm, a modulus of elasticity of 46.2 GPa, an ultimate tensile stress

of 850 MPa, and an ultimate strain of 1.9%. Six coupons were tested in direct tension to obtain these average values.

Table 2. Physical characteristics and properties of badminton fibres

l_F (mm)	d_F (mm)	l_F/d_F	$f_{t,F}$ (MPa)	F (GPa)	ρ_F (kg/m^3)
25	0.68	36.76	575 (22.4)	5.8 (26.4)	1250

Note: l_F = fibre length, d_F = fibre diameter, l_F/d_F = aspect ratio, $f_{t,F}$ = tensile strength, E_F = modulus of elasticity and ρ_F = fibre density.

Post-Tensioned Metal Straps (PTMS). A different number of straps (n=1, 2 or 3) was placed parallel to the bench, with a spacing of 100 mm at centres. The straps used in the post-tensioning system had a cross-section of 32×1.0 mm (width×thickness). The force on the straps was applied using a pneumatic tensioner calibrated to a pressure of 8 bar (i.e. 116 psi), as explained later. Average yield stress (850 MPa) and ultimate stress (950 MPa) were obtained from six strap coupons. The elongation at rupture of the metal straps was 9.6%.

2.2.3 Concrete mixes

Table 3 summarises the proportions of the RAC mixes, which were produced using CEM II and with the total replacement of aggregates with RCA. The RCA was used directly in the mix without pre-soaking or surface pre-treatment, which proved to be cost-effective. Five RAC mixes were produced to evaluate the optimum dosage of fibres (F) considering volume fractions of fibres from 0.5% and up to 2.0%. The mix details are listed in **Table 3**. The RAC mix was designed following ACI 211.1 [34] and had recycled coarse and fine aggregates, as well as a water / cement (w/c) ratio of 0.55. The original RAC mix was designed for a target compressive strength of 35.0 MPa and a slump equal to 80 mm. Superplasticiser (SP) measured by volume was added into the mixes with fibres to improve their workability. However, the proportions of superplasticiser and water were slightly varied in each RAC mix to consider the RCA's higher water absorption.

Table 3. Mix design of RAC with different amount of racquet fibres (amounts per m^3)

Concrete mixes	CEM II (kg)	Fine RF (kg)	Coarse RC (kg)	Water + SP	Slump (mm)	Silica fume (kg)	Racquet fibres (%)
RAC	357	840	864	195	80	5	0
RAC+0.5F	357	840	864	195	75	5	0.5
RAC+1.0F	357	840	864	195	76	5	1.0
RAC+1.5F	357	840	864	195	70	5	1.5
RAC+2.0F	357	840	864	195	70	5	2.0

Table 4 shows the (hardened) mechanical properties of the mixes. The average compressive strengths (f_{cm}) were obtained from three cylinders of size ⌀150×300 mm, tested according to ASTM C39 [35]. Likewise, the tensile strength (f_t) was obtained from three cylinders of size ⌀150×300 mm according to ASTM C496 [36]. The modulus of rupture (f_b) was obtained from three 100×100×500 mm prisms, according to ASTM C78 [37]. **Fig. 4** compares average stress-strain relationships from cylinders tested in compression. The strains in the cylinders were measured with foil-type strain gauges glued vertically to the cylinders' surface. The results in **Table 4** indicate that mix RAC has the highest f_{cm} and the lowest axial strains. As larger volumes of fibre are added to the mixes, the value of f_{cm} reduces, whereas the axial strains increase progressively. The reduction in f_{cm} can be potentially due to the air (voids) induced during mixing owing to the presence of the fibres. However, it should be noted that compared to mix RAC+0.5F, mix RAC has lower tensile splitting and modulus of rupture strengths (approximately 8% and 10% respectively). The higher values of f_t and f_b as well as the higher strains in RAC with fibres (range from 2800 - 3600 microstrains) are attributed to bridging effects given by the fibres acting between cracks, which in turn increase the RAC's deformability. The results in **Fig. 4** are later utilised for a numerical analysis.

The experimental results in **Table 4** also indicate that the maximum and splitting tensile and modulus of rupture strengths were for mix RAC+1.5F (f_t = 4.8 MPa and f_b = 4.3 MPa, respectively). It is

also shown that, whilst the strength parameters increased with the addition of fibres (up to a volume of 1.5%), the strengths started reducing when the volume of fibres increased to 2% (see mix RAC+2.0F). This could be attributed to balling effects of the racquet fibres at such relatively high-volume fraction. The modulus of rupture and splitting tensile strengths of mix RAC+1.5F were about 41.2% and 38.7% higher, respectively, over the RAC mix without fibres. In view of these results, it was considered that mix RAC+1.5F contained the maximum feasible dosage of racquet fibres, and thus only mixes with volumes of 0.5%, 1.0% and 1.5% were used to cast the cantilever benches in Series I. It should be noted that whilst the tests in this section prove that the fibres enhance the tensile strength of RAC, additional research is needed to investigate in more detail the bond behaviour between individual racquet fibres and the concrete interface.

Table 4. Mechanical properties of RAC and RAC with racquet fibres at 28 days

Concrete mixes (different fibre content)	Axial strain (microstrains)	f_{cm} (MPa)		f_t (MPa)		f_b (MPa)	
		Mean	SD	Mean	SD	Mean	SD
RAC	2600	41.1	4.9	3.1	0.47	3.4	0.56
RAC+0.5F	2750	35.9	4.08	3.4	0.42	3.8	0.50
RAC+1.0F	3160	33.8	4.03	3.7	0.41	4.2	0.48
RAC+1.5F	3390	30.7	4.29	4.3	0.48	4.8	0.55
RAC+2.0F	3600	29.9	4.41	3.9	0.42	4.4	0.49

Note: f_{cm} = cylinder compressive strength, f_t = tensile splitting strength, f_b = flexural strength of prism, SD = standard deviation.

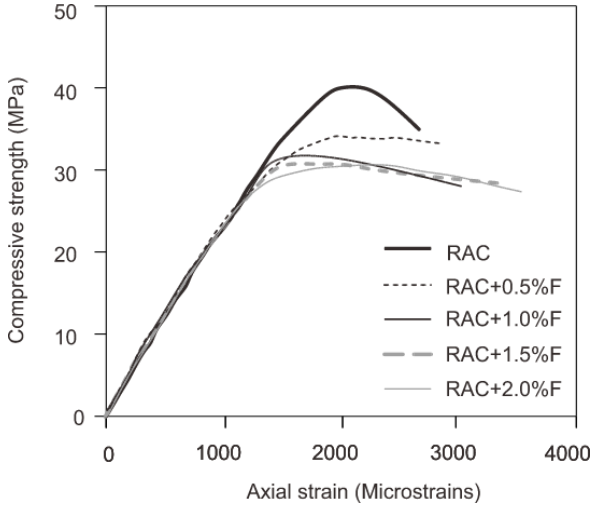

Fig. 4. Stress-strain relationship of RAC mixtures with different fibre volume fractions.

2.3 Construction of bench specimens

2.3.1 Series I

Twelve benches (**Fig. 5a**) were cast with 100% RAC reinforced with racquet fibres. Initially in Series I, three cantilever benches were cast for each volume fraction of fibres ranging from 0.5% to 1.5%, as well as three control RAC benches. Ad-hoc moulds were produced to cast the benches. After placing the GFRP bars, the RAC was cast into the moulds. Care was taken to guarantee a uniform distribution of fibres throughout the concrete mix during mixing. The moulds were then vibrated to remove any air pockets and to ensure compaction. The moulds were removed after 24 h, after which the benches were cured for 28 days using wet jute bags.

2.3.2 Series II: Post-tensioned RAC benches

In Series II, nine cantilever benches were cast but only with mix RAC+1.5%F. Additionally, PTMS were used as post-tensioning reinforcement adopting 1, 2 or 3 straps (see Section A-A in **Fig. 5b)**. Before casting the concrete, the metal straps were positioned within the moulds to allow for subsequent post-tensioning. Openings left at the top part of the benches exposed the metal straps, as shown in **Fig. 6a**. After 28 days, a pneumatic tensioner tool was used to apply force to the metal straps (**Fig. 6b**). To

keep the tension force in place, the straps were clamped with metal clips using pneumatic jaws. The openings were eventually filled in with mortar.

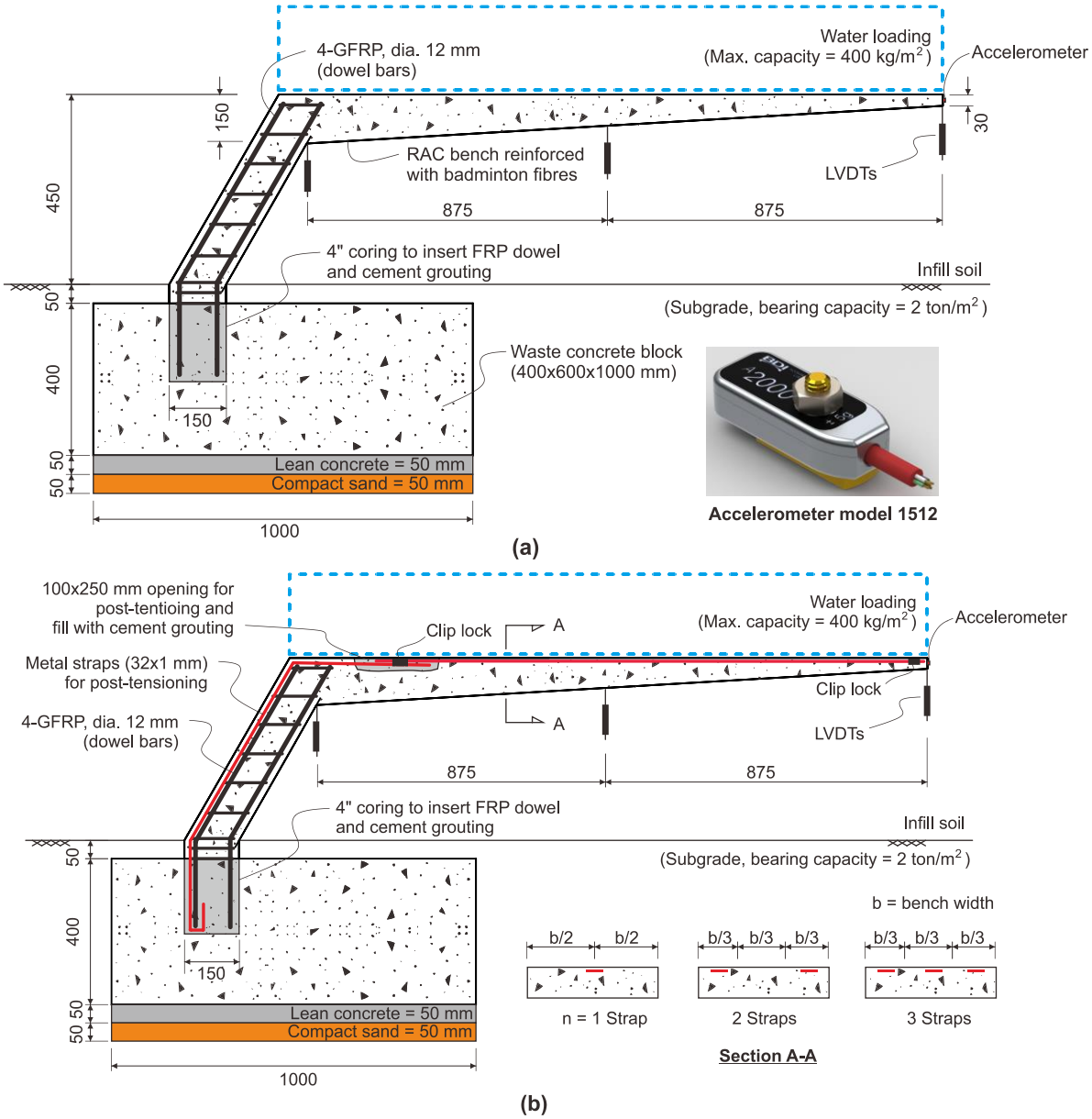

Fig. 5. Details of benches: (a) Series I, and (b) Series II: PTMS benches (units: mm).

(a) (b)

Fig. 6. Post-tensioning of metal straps in benches Series II (n=3): (a) openings left to apply post-tensioning, and (b) application of post-tensioning with tensioner tool.

2.4 Test setup and instrumentation

Short-term flexural tests. The load was applied using water tanks that induced a stress of 400 kg/m^2 (3.92 kN/m^2) on the bench, as shown in **Fig 7a**. Three Linear Variable Displacement Transducers (LVDTs) under the bench measured vertical deflections, including one at the bench tip.

Long-term flexural tests. A static load was applied using concrete blocks of 300 kg/m^2 (2.94 kN/m^2) placed on the bench (**Fig. 7b**). Three LVDTs were used in measuring the deflections over a period of 365 days. After 365 days, the concrete blocks were taken off the bench. The deflections were then monitored for another 30 days after removing the blocks. After the period of 365 days, and following the removal of the blocks, the measurement of deflections continued for 30 days.

Fig. 7. Test setup and instrumentation of: (a) short-term flexural tests, (b) long-term flexural tests, (c) female and (d) male walking scenarios.

Table 5. Acceleration effects [39] on human perception of vibration

Human perception effect	Range of accelerations
Imperceptible	$a < 0.005$g
Perceptible	$0.005 \leq a \leq 0.015$g
Annoying	0.015g $\leq a \leq 0.05$g
Very annoying	0.05g $\leq a \leq 0.15$g
Intolerable	0.15g $< a$

Human-induced vibration tests. There are presently no guidelines that cover human-induced vibration tests of urban furniture. Therefore, BS 6472-1 [38] and ISO 2631-2 [39] are adopted here to serve as a reference for the tests involving human-induced vibrations. The acceleration values reported in Table 5 are felt by occupants of a floor in a building, which is assumed to be analogue to the sitting area of the bench. ISO 2631-2 [39] sets an average perception limit of 0.015 m/s ²for a group of fit and alert occupants. As a result, occupants of floor buildings are likely to feel accelerations above 0.015 m/s ². For these tests, a 77 kg treadmill was placed on top of the benches to carry out the tests. A male and a female participant with a mass / height of (respectively) 58 kg / 177 cm and 54 kg / 160 cm were instructed to use the treadmill. The three case scenarios considered were: normal walking (average walking speed =5 km/h), brisk walking (average walking speed = 10 km/h) and jumping. The maximum vibrations (accelerations) were measured as a fraction of gravity following BS 6472-1 [38]. To achieve

this, a triaxial accelerometer (model BDI A2000) of capacity ± 5.0g was placed underneath the tip of the benches, as shown in **Figs. 5a-b**. A view of the human-induced vibration tests is shown in **Figs. 7c-d**. The values in **Table 5** are later compared with experimental results obtained from the human-induced vibration tests on the bench.

3 Test results and discussion

3.1 Short-term loading

Fig. 8a shows a typical load vs bench tip deflection of benches with RAC and fibre volume fractions of 0%, 0.5%, 1.0% and 1.5%. The results show that the load consistently increases in benches cast with RAC with fibres over the control benches without fibres. After the initiation of cracking, there is no significant increase in load nor displacement in the control bench RAC without fibres, resulting in a brittle failure. The load-deflection curves show that the load and ductility of the benches with fibres increased with an increment of fibre volume fraction. The addition of fibres in volumes of 0.5%, 1% and 1.5% also increased the flexural capacity of the benches by 77%, 90% and 101%, respectively, when compared to the control bench. The addition of fibres also enhanced stiffness and ductility of the fibres added to the bench. Indeed, the maximum increase in displacement (+101%) was for the bench with RAC and 1.5% volume fraction of fibres over that of the bench without fibres. Also, the propagation of micro-cracks into the macro-cracks was restrained by the incorporation of the high volume of fibres into the RAC bench. Overall, curves in **Fig. 8a** suggest that the bench with RAC and 1.5% volume fraction of fibres can be considered as the optimised solution in Series I.

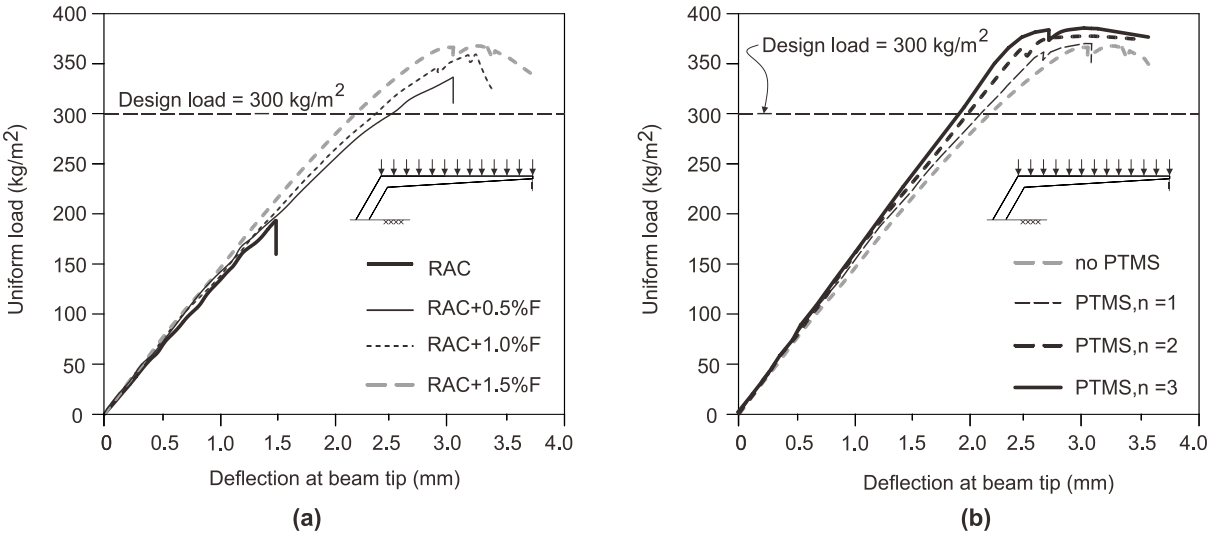

Fig. 8. Short-term flexural test results: (a) RAC benches with different fibre contents (Series I), and (b) RAC benches with 1.5% fibre contents and PTMS (Series II).

In Series II, the benches were made with RAC and 1.5% of fibres, was well as with 1, 2 or 3 post-tensioned metal straps. A similar procedure was followed as Series I to study the effect of PTMS with different layers using the optimised content of fibres. **Fig. 8b** compares the load vs bench tip deflections of benches with PTMS (n=1, 2 or 3 layers). **Fig. 8b** indicates that the load increased with the increase in PTMS layers. This is because the applied compressive stress in the concrete, which counteracted the tensile stresses at the top of the bench. The increase in load for benches with PTMS was about 103%, 110% and 113% with layers n=1, 2 and 3, over control benches without fibres and without PTMS. The flexural strength of the benches with 1, 2 or 3 PTMS layers was enhanced by about 1.1%, 4.3% and 5.7% when compared with the bench with a volume of 1.5% of fibres. This can be attributed to the addition of both fibres and PTMS, which reduces the flexibility of the bench and prevents brittle failures. The increase in PTMS layers from n=2 to n=3 increased the load capacity of the bench only marginally (+1.3%), which was not cost-effective. Hence, it is recommended to build the cantilever bench with a maximum of 2 layers of PTMS and RAC with racquet fibres.

3.2 Long-term loading

Figs. 9a-b show the results obtained from the sustained load conducted over 365 days. **Fig. 9a** compares the uniform load vs bench tip deflection without and with PTMS (n=1, 2 and 3). The test results reveal that the deflection decreased with increasing number of PTMS layers. Also, there was a significant improvement in the deflection behaviour of PTMS (bench with n=3) when compared to the control bench. This can be attributed to the additional stiffness provided by the post-tensioned metal straps, which provide active confinement to the sitting area of the benches. The experimental results also show a marginal improvement in behaviour if the number of PTMS layers increases from 2 to 3 (see n=2 and 3), as evidenced by a load increase of 11% over the bench with 2 layers of PTMS.

Fig. 9b shows the maximum deflections (Δ_{max}) and residual deflections (Δ_r) recorded in the benches. Compared to the RAC bench with 3 layers of PTMS (n=3), the Δ_{max} and Δ_r of the control bench without PTMS was 27.2% and 63.3% higher, respectively. Accordingly, it is possible to conclude that the urban cantilever bench can be manufactured with the addition of 1.5% racquet fibres and 2 layers of PTMS confinement to keep the structure cost-effective and constructively feasible.

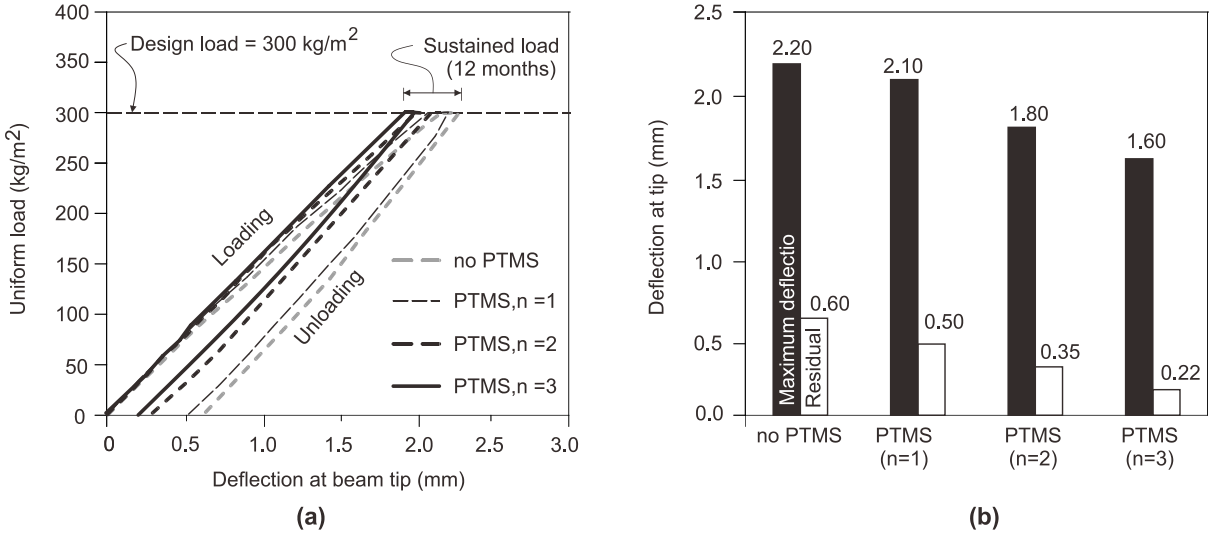

Fig. 9. Results from 365-day sustained loading tests (a) load vs bench tip deflection, and (b) maximum and residual bench tip deflection for benches with and without PTMS.

3.3 Vibration performance

3.3.1 Bench accelerations

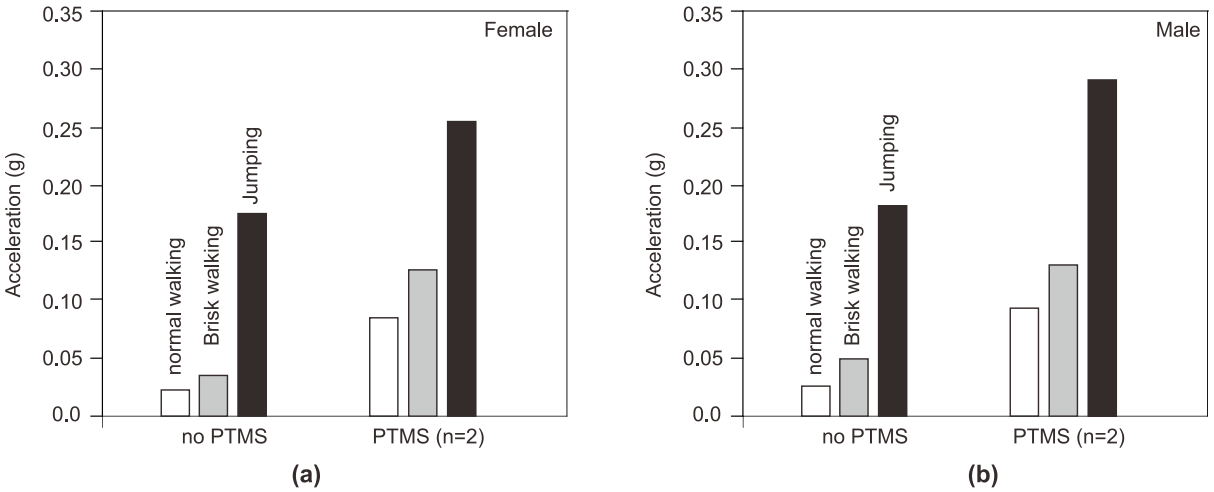

Fig. 10. Vibration test results on the maximum acceleration to normal walking (white), brisk walking (gray), and jumping (black): (a) female and (b) male cases.

Figs. 10a and 10b compare the maximum accelerations of the benches with and without PMTS for the three scenarios (walking, brisk walking, as well as jumping) for female and male cases. The

results in **Figs. 10a-b** show that, in the case of the PTMS bench, the acceleration tended to increase by about 42% with the walking speed of the participant. As for jumping, the acceleration of the benches was above the "irritating" level (refer to **Table 5**). Overall, the use of RAC led to higher accelerations during the three considered scenarios. Compared to the RAC bench with PTMS, the acceleration of the RAC bench without PTMS for increased for normal walking (24.3%), brisk walking (8.3%) and jumping (17.5%). In spite of this, the vibration of the benches was below the ISO 2631-1 [40] and BS 6472-1 [38] limits. This confirms that the vibration performance of the benches was within the limits imposed by guidelines.

3.3.2 Natural frequency

ISO 2631-1 [40] and BS 6472-1 [38] state that a floor should have a natural frequency higher than 8.0 Hz to remain within standard vibration levels, mainly because occupants could feel vibration discomfort at lower frequencies. Fourier analyses were performed in Matlab® using the frequency responses from the vibration results on the benches. From the test results, it is evident that the PTMS used in the benches changed the vibrations. Specifically, for normal walking, the vibration increased by 24.3% for the bench without PTMS when compared to the PTMS bench. During brisk walking, the vibration increased by 8.3%. Similarly, for jumping, the vibration increased by 9.3%. The frequency results for RAC benches with or without PTMS show that, for both male and female participants, the natural frequencies for normal walking (5.11-6.75 Hz), brisk walking (8.47-9.23 Hz) and jumping (9.69-11.74 Hz) were within acceptable limits of occupants' comfort. Consequently, RAC is considered as a feasible option for the construction of urban furniture. The vibration levels experienced during human-induced activities were found to be within an acceptable limit, indicating satisfactory serviceability conditions if users use the benches to exercise. It should be noted that, in the analysis described in this section, only 60 s of data were considered.

3.4 Effect of the number of metal straps and optimised solution

Overall, the incorporation of PTMS in the benches tested in Series II enhanced the structural performance of the benches compared to Series I. By introducing compressive stresses in the cross section through the metal straps, the tensile forces in the RAC benches were effectively counteracted, significantly increasing stiffness and load-bearing capacity. Indeed, the experimental results showed an 83% reduction in deflections for the benches in Series II over Series I counterparts (see **Fig. 8b**), thus confirming a substantial improvement in flexural rigidity. This enhancement is crucial for cantilever structures, which inherently experience large deflections at their free ends. The post-tensioning also improved the vibration characteristics of the benches. The natural frequencies of benches in Series II were 93.3% lower compared to their non-post-tensioned counterparts in Series I. The increased stiffness made the benches less prone to resonant vibrations under dynamic loading, which is vital for public furniture where user comfort and structural integrity are relevant.

The static test results also proved that the capacity of a PTMS bench with 3 layers is only 1.3% higher than that of benches with 2 layers. Hence, the use of 2 layers of metal straps for post-tensioning in Series II proved to be both efficient and cost-effective. The labour and material cost to install one layer of PTMS is about $5 USD at 2024 prices. Hence, it is suggested to use 2 straps PTMS with mix RAC+1.5F to manufacture the benches. Overall, the simplicity of installing and adjusting the metal straps off-site makes the PTMS approach feasible for large-scale production and practical applications, particularly in urban infrastructure.

4 Numerical study

4.1 Geometry and concrete models

To gain deeper insight into the benches' performance, nonlinear finite element analyses (FEA) were conducted using Abaqus®. Material and geometric nonlinearities were considered in the analyses. For all benches, 8-node brick elements (type C3D10M) were used to model the concrete, as shown in **Fig. 11a**. The concrete base was modelled with solid elements type C3D8R, adopting a modified second-order integration scheme. A mesh size of 8 mm was chosen based on an optimisation mesh sensitivity analysis in Abaqus®. The model had a total of 347,412 elements, as well as 318,560 nodes.

The load was defined in 8 steps (equivalent to 50 kg/m^2 of water increment during the field load test), in the form of applied pressure, which was applied directly on the top surface of the bench to simulate the actual field load test with the increment of 50 kg/m^2 (0.00049 MPa), see **Fig. 11b**. The Abaqus® analysis was halted at a pre-determined number of steps, defined based on the maximum load recorded. This corresponds to a maximum applied load of 400 kg/m^2 (or 0.0039 MPa). Previous research [41] proved that such approach was accurate for numerical evaluations of the serviceability behaviour (e.g. crack widths and deflections) of concrete with fibres. As such, it should be noted that the analysis focused primarily on the service behaviour of the benches (i.e. SLS), not on the ultimate limit state (ULS). The deflection values at the tip of the bench were recorded at each load step to obtain the discrete load vs. deflection curve. The concrete base was modelled as a pinned boundary condition to simulate actual field conditions (**Fig. 11b**).

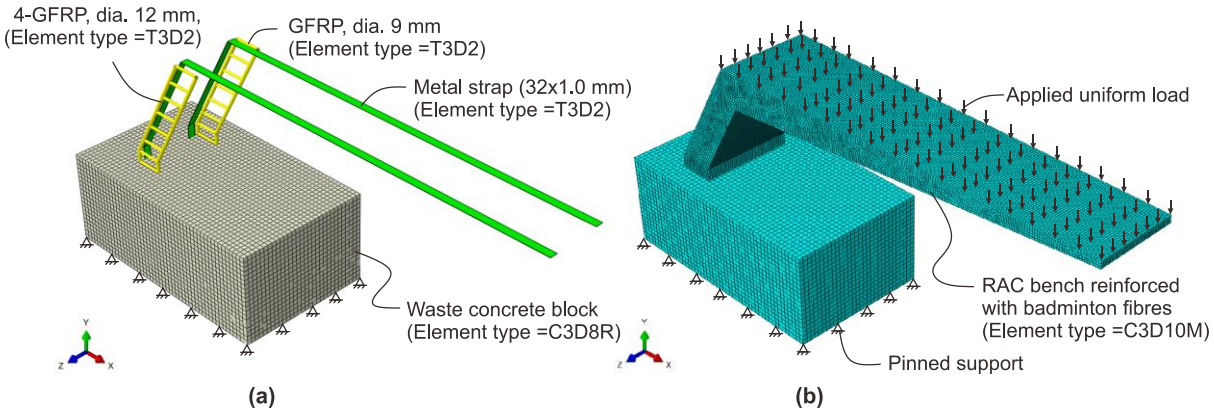

Fig. 11. 3D meshing in FE model: (a) FRP reinforcement (linear truss element) and metal strap (linear truss element) embedded in concrete, and (b) components with applied pressure.

4.2 Material constitutive models

Concrete constitutive model. The properties of RAC obtained from the experimental results summarised in Section 2.2.4 were adopted here. The numerical analyses in Abaqus® adopted a concrete damaged plasticity (CDP) model, which has proven to be satisfactorily accurate to simulate the bending and shear behaviour of concrete elements [42, 43]. **Figs. 12a-b** show schematically the uniaxial constitutive models of the RAC with 1.5% racquet fibres, both in compression and tension respectively. Note that the test values of stress-strain shown in **Fig. 4** were adopted for modelling. The stress-strain relationship in uniaxial compression (see **Fig. 12a**) was linear up to the initial yield point, σ_{c0}. In this plot, the value σ_{c0} represents the point where the concrete deviates from its initial linear elasticity [44]. Point σ_{c0} is typically marked by the onset of microcracking in the concrete matrix, thus resulting in a nonlinear stress-strain relationship. After σ_{c0}, the concrete keeps experiencing strain under higher applied stresses (but with a lower stiffness) until failure. The plastic zone of the relationship was assumed as having stress hardening until the ultimate stress σ_{cu}, subsequently followed by strain softening after such ultimate stress. The stress-strain relationship in uniaxial tension (see **Fig. 12b**) was considered as linear-elastic up to the stress at failure $\sigma_{t0,}$ which marks the onset of microcracking in tension. After σ_{t0}, the development of cracks in the tension zone is simulated by a softening stress-strain behaviour.

To ensure results which are independent of the mesh, the descending branch in **Fig. 12a** was calculated with the formulas in reference [45]. In the same manner, the nonlinear descending portion of the tensile stress-strain curve (**Fig. 12b)** was calculated adopting the stress-crack opening formulation suggested in [46]. **Fig. 12a** includes a compressive damage parameter defined by D_c, or the ratio between the inelastic strain and the total strain**.** **Fig. 12b** also includes an analogue tensile damage parameter D_t, which is defined as the ratio of the cracking strain to the total strain. In this article, an exponential function was adopted to calculate D_c and D_t. Other analysis parameters of the CDP material model are as follows: dilation angle of 40 °, eccentricity value of 0.1, ratio f_{b0}/f_{c0} of 1.17, as well as K = 0.666. Concrete has a softening behaviour and stiffness degradation, which can result in convergence

issues. Accordingly, a viscoelastic regularisation technique (with a viscosity parameter μ = 0.001) was implemented in the CDP model to let stresses fall outside of the yield surface. This parameter was used successfully to study the deformation of GFRP RAC elements with fibres in a previous study by the authors [41].

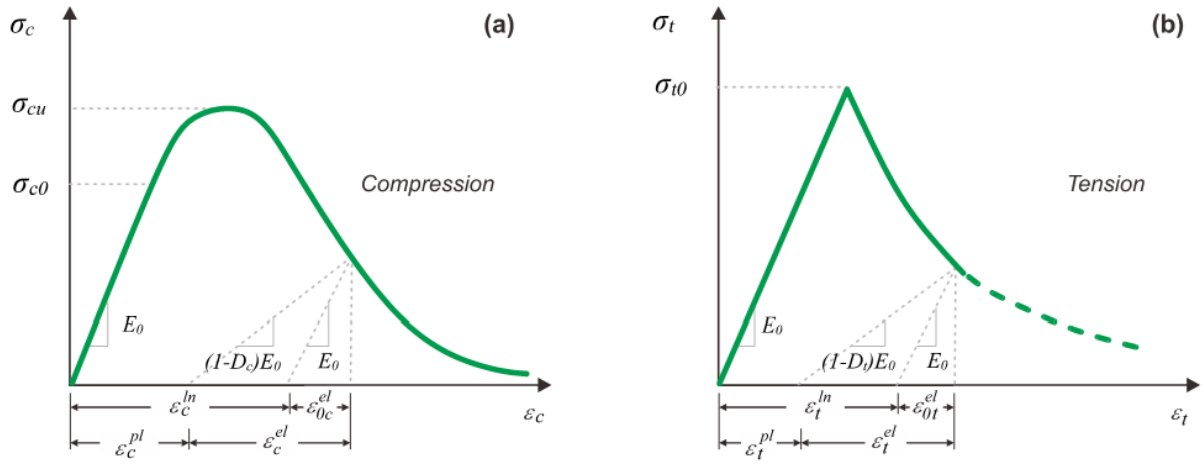

Fig. 12. Constitutive stress-strain models of RAC+1.5%F mix used in finite element analyses (a) uniaxial compression, (b) uniaxial tension [44].

FRP bars and Post-Tensioned Metal Straps. The GFRP dowel bars and metal straps were modelled with 2-node truss elements (type T3D2), including two Gauss-Legendre integration points (see **Fig. 13a**). The stress-strain behaviour of both GFRP bars and metal straps was assumed to be linear. The analysis focused on analysing deflections and stresses at SLS, and thus perfect bond was assumed between the reinforcement (GFRP dowels and metal straps) and the surrounding concrete (both in the concrete base and bench). This was also considered reasonable since no bond failures were observed in the tested benches. For the metal straps, the strengths and modulus of elasticity obtained from the tests were given to the FE model, i.e. f_y = 800 MPa, f_u = 950 MPa, E = 2.1 ×10^5, and ν = 0.3. To simulate the tension force on a metal strap embedded in a concrete bench, an iterative approach was adopted to find a temperature value that induced the actual tension force of 350 MPa applied to every single strap, as previously reported by the authors [21].

Racquet fibres. The presence of the fibres in RAC was considered using a direct tension force transfer model, as suggested in [47]. Thus, the fibres are treated as direct force transfer elements within the RAC (**Fig. 13a**). The model in [47] can account for different bond stresses (τ_u) of other types of fibres (e.g. racquet string fibres) with different geometries. It can also consider the dominant pull-out failure mechanism across crack interfaces when debonding occurs between concrete and fibres at the maximum bond stress (τ_{max}). Several fibres are deemed to resist tensile stresses in a direction perpendicular to a crack, as a function of the diameter of a fibre (φ_{sf}) and the volume fraction V_f (see **Fig. 13b)**, If it is assumed that the fibres are fully bonded to the RAC before pulling out (**Fig. 13c**), then the maximum stress in the fibres ($\sigma_{sf,max}$) when the bond stress reaches the interfacial bond stress (τ_{max}) can be computed with Eq. (1).

$$\sigma_{sf,max} = \frac{0.41 V_f \tau_{max} L_f}{\varphi_{sf}} \quad (1)$$

where the interfacial bond stress is $\tau_{max} = \tau_u d_f$; τ_u = bond strength between fibre and concrete; d_f = shape factor of the fibre (d_f=0.5 for racquet fibres); L_f = fibre length; V_f = fibre volume fraction; and φ_{sf} = fibre diameter.

The authors developed an ad-hoc Python script subroutine in Abaqus® to randomly distribute the racquet fibres within the RAC [41]. A sphere was assumed around each fibre (in a 3D space) to prevent intersections between fibres. Likewise, to facilitate the fibre distribution, a random function was adopted to define the coordinates of the fibres' centre, as well as for the fibres' orientation. The following parameters were defined for each fibre in the Python code:

$$fibre = [X_{cf}, Y_{cf}, L_f, \alpha_f, \varphi_{sf}] \quad (2)$$

where X_{cf}, Y_{cf} = x and y coordinates of the centre of the fibre; L_f = fibre length; α_f = orientation angle of the fibre; and φ_{sf} = fibre diameter.

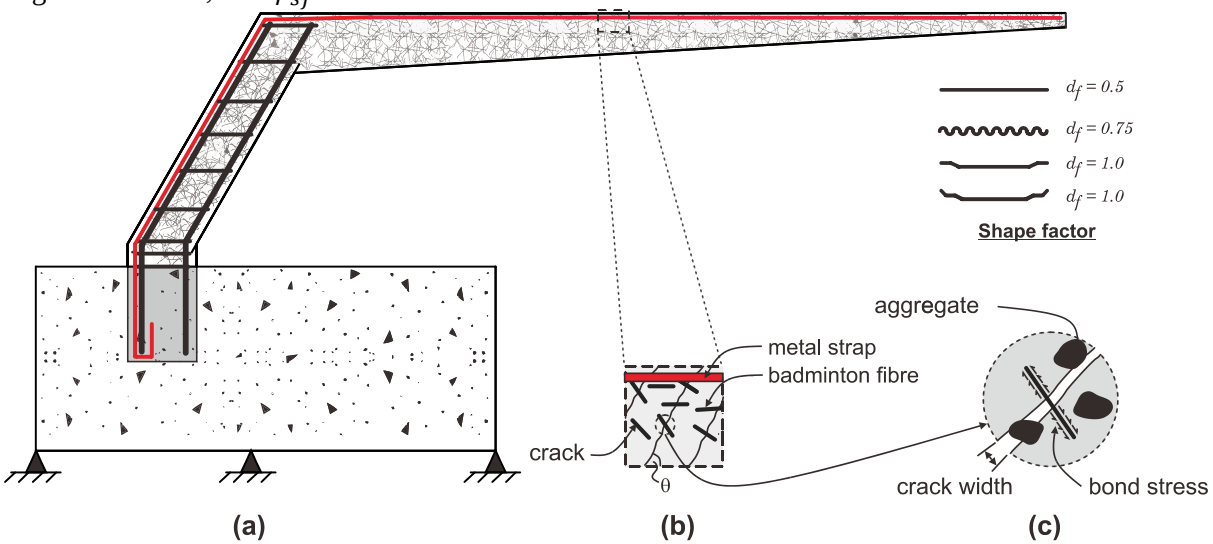

Fig. 13. Direct tension force transfer mechanism of racquet fibres across cracks: (a) fibres in RAC, (b) fibres across opening cracks, and (c) single fibre with bond stress across inclined.

In predicting the bench deflections, the Abaqus® analyses were terminated at predefined load steps based on the maximum experimental results. Previous research [41] confirms this method is sufficiently accuracy for evaluating the crack widths and deflections of FRP reinforced concrete elements with fibres. However, this modelling approach should not be generalised to other cases until further numerical evidence is available.

4.2 Comparison of experimental results and FEA predictions

4.2.1 Damage and short-term deflections

A damage index analysis of concrete was carried out by defining compressive (DAMGEC) and tensile (DAMGET) damage in Abaqus®. Accordingly, cracking is deemed to develop in the concrete once the magnitude of DAMGET is higher than 1.0. **Figs. 14** and **15** show the cracking pattern at service load (P=400 kg/m^2) of the RAC benches tested in Series I and II, respectively. The results obtained from the Abaqus® models (FEA) match well the experimental (EXP) observations as reported in **Table 6**, where the deformations from the static loading tests (Section 3.1) are included. **Table 6** also reports the error (in %), which indicates the precision of the ultimate load and deflection at the bench tip, as calculated by Abaqus®. The results in **Table 6** show that, in general, the FEA predictions match well (accuracy between 2 - 5%) the experimental results, therefore suggesting that Abaqus® can simulate reasonably well the behaviour of the benches.

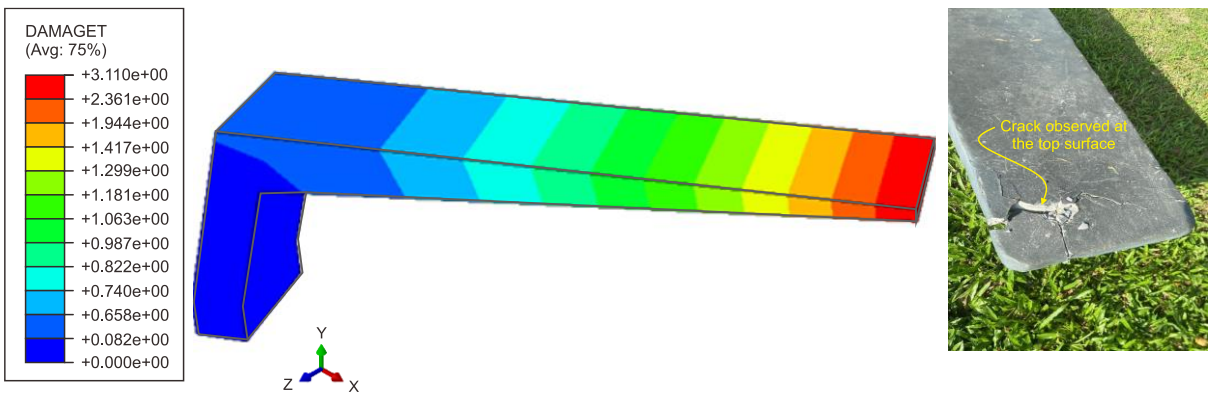

Fig. 14. DAMGET crack analysis results of bench RAC+1.5%F without PTMS (Series I) at service load.

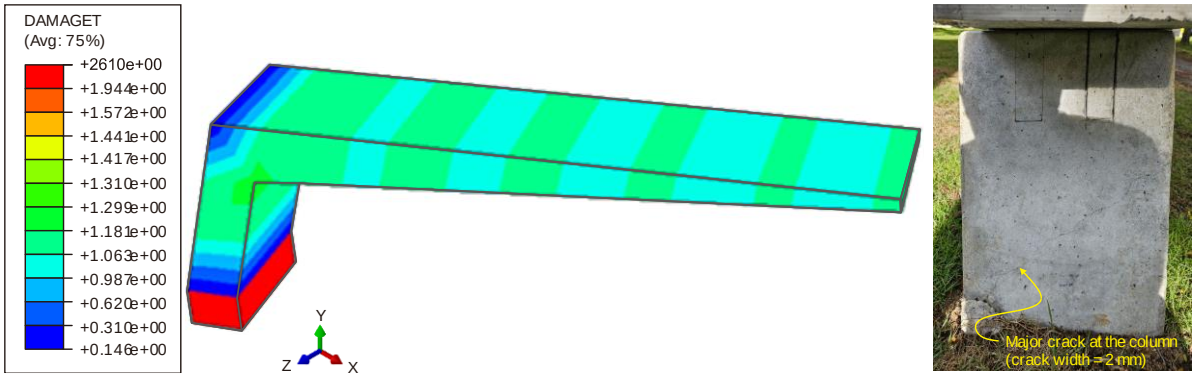

Fig. 15. DAMGET crack analysis results of bench RAC+1.5%F with PTMS (Series II) at service load.

Table 6. Comparison of experimental and FEA results of short-term load test at service load (P=400 kg/m^2)

Bench ID	Deflection at tip of bench (mm)		Error %
	EXP	FEA	
RAC+1.5%F	3.04	3.11	2.3
RAC+1.5%F with PTMS (n=2)	2.50	2.61	4.4

4.2.2 Long-term flexural test analysis

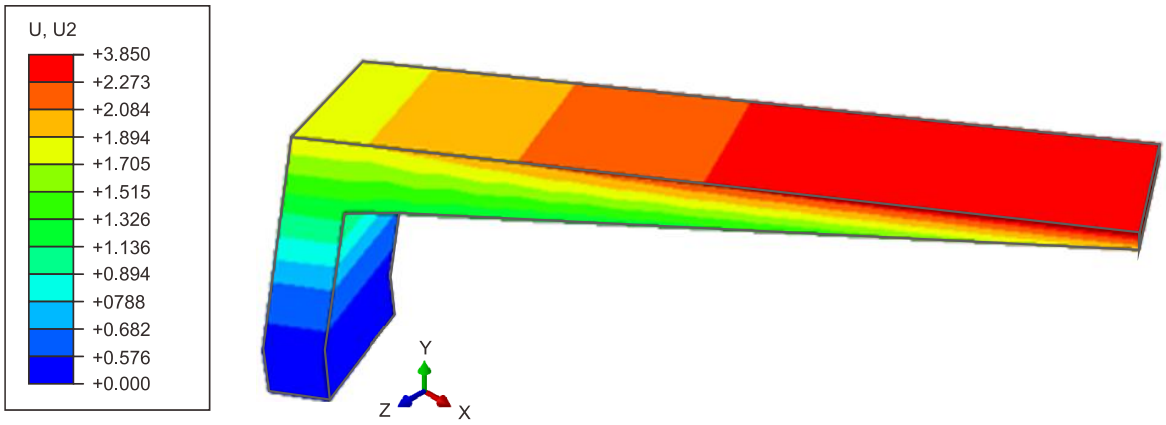

Fig. 16. Long-term loading analysis results of bench RAC+1.5%F without PTMS (Series I) at service load.

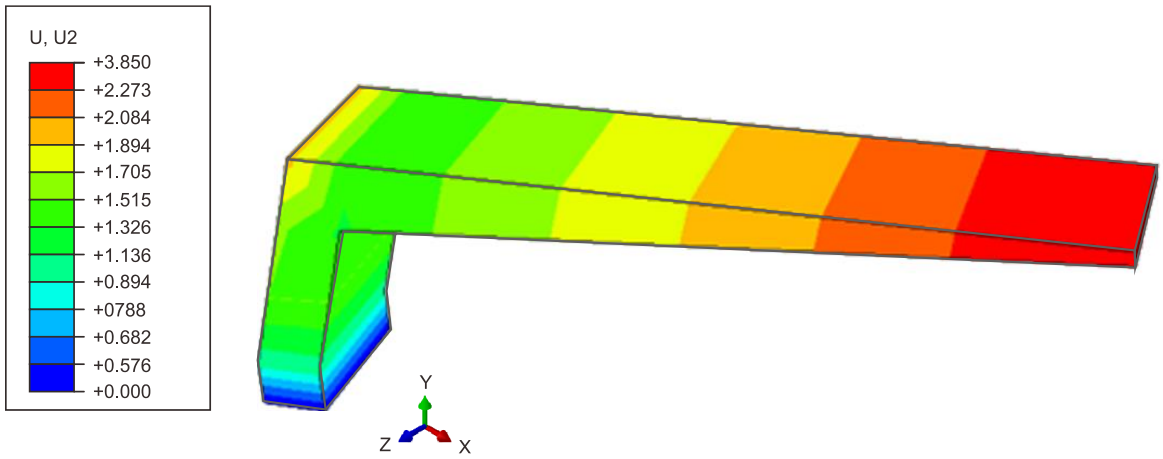

Fig. 17. Long-term loading analysis results of bench RAC+1.5%F with PTMS (Series II) at service load.

Figs. 16 and **17** compare the long-term deformations in the RAC benches without (Series I) and with PTMS (Series II), respectively. **Table 7** also compares maximum loads and corresponding bench tip deflections recorded in the experiments (EXP) and those calculated by Abaqus® (FEA). The table also includes the error in %. The results in **Table 7** show that, in general, the Abaqus® predictions

match well (within 1 to 3%) with the experimental results, which in turn suggests that Abaqus® can simulate well the long-term behaviour of the benches.

Table 7. Comparison of experimental and FEA results of long-term loading (P=300 kg/m^2) after 365 days

Bench ID	Deflection at tip of bench (mm)		Error %
	EXP	FEA	
RAC+1.5%F	3.74	3.85	2.9
RAC+1.5%F with PTMS (n=2)	3.13	3.17	1.3

4.2.3 Natural frequency

Figs. 18 and **19** compare the results obtained from the frequency analysis, modal shapes and first mode natural frequencies. The first natural frequency of the benches were 6.81 Hz and 5.19 Hz for the bench with (Series II) and without PTMS (Series I) respectively. The results from the FEA indicate that the models calibrated in Abaqus® can simulate well the dynamic characteristics of the tested benches.

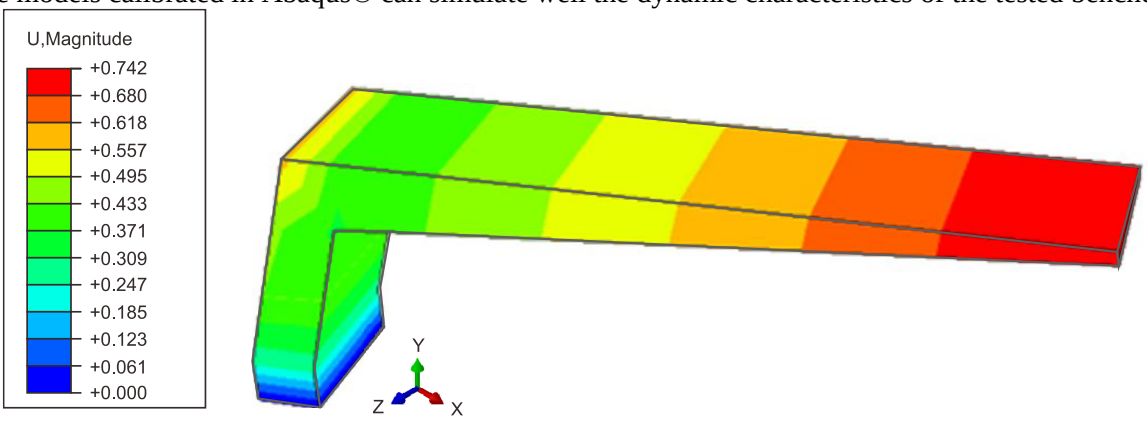

Fig. 18. Modal shape of bench RAC+1.5%F without PTMS (Series I), f_1=5.19 Hz.

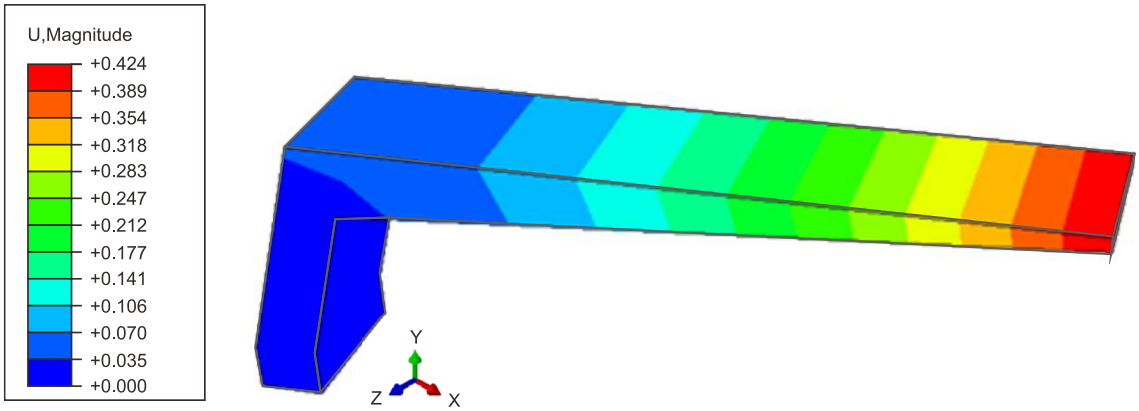

Fig. 19. Modal shape of bench RAC+1.5%F with PTMS (Series II), f_1=6.81 Hz.

5 Analytical study on fatigue life

This section examines the fatigue performance of RAC structures under fatigue loading by considering the bench as a post-tensioned cantilever bench (i.e. with PTMS) under a load distributed at the top. Accordingly, the maximum stress at the base is given by Eq. (3).

$$\sigma_{max} = \frac{M_{max} y}{I} \tag{3}$$

where M_{max} = maximum bending moment at the base, y = distance from the neutral axis (half of the thickness at the base), and I = moment of inertia of cross section.

The maximum bending moment for a load P at the free end of a cantilever beam of length L is given by Eq. (4).

$$M_{max} = PL \tag{4}$$

The moment of inertia (i.e. second moment of area) of a rectangular cross-section of width *b* and height *t* is shown in Eq. (5).

$$I = \frac{bt^3}{12} \tag{5}$$

Accordingly, the stress at the base becomes σ_{max}, as defined by Eq. (6):

$$\sigma_{max} = \frac{P\,L(t_b/2)}{\frac{b\,t_b^3}{12}} = \frac{6PL}{bt_b^2} \tag{6}$$

A time-dependent degradation factor, *D(t),* is incorporated here, which represents the reduction in the fatigue strength over time. This factor is usually modelled exponentially by Eq. (7):

$$D(t) = e^{-\beta t'} \tag{7}$$

where, β is the degradation rate (a constant), *t* is the specimen thickness and t' is the time.

The fatigue strength of the material degrades over time (t') and can be calculated using Eq. (8):

$$\sigma_f\,(t') = \sigma_{f0} D(t') \tag{8}$$

where, σ_{f0} is the initial fatigue strength.

Basquin's equation with time-dependent fatigue strength is shown in Eq. (9) and Eq. (10).

$$\sigma_{max}^a N_f D(t') = C \tag{9}$$

Substituting Eq. (6) into Eq. (9), results in:

$$\left(\frac{6PL}{bt_b^2}\right)^a N_f e^{-\beta t'} = C \tag{10}$$

Solving for N_f , the fatigue life can be expressed as

$$N_f = \frac{C}{\left(\frac{6PL}{bt_b^2}\right)^a e^{-\beta t'}} \tag{11}$$

The predicted fatigue life (N_f) of the cantilever bench is shown in Eqs. (12a-b), considering time-dependent degradation:

$$N_f = \frac{Cb^a(t)^{2a}}{(6PL)^a e^{-\beta t'}} \tag{12a}$$

Or alternatively:

$$N_f = \left(\frac{Cbt^2}{6PL}\right)^a \cdot e^{\beta t'} \tag{12b}$$

The fatigue life coefficients were calculated assuming a fatigue strength exponent a = 0.3585, a fatigue strength coefficient C = 12000, and a degradation rate value $\beta \approx 0.00195$ day^{-1} [30]. These serve as input in the fatigue life prediction equation to assess the theoretical long-term behaviour of the cantilever RAC bench. Detailed calculations of the theoretical fatigue life prediction of a RAC cantilever bench are presented in **Appendix B**.

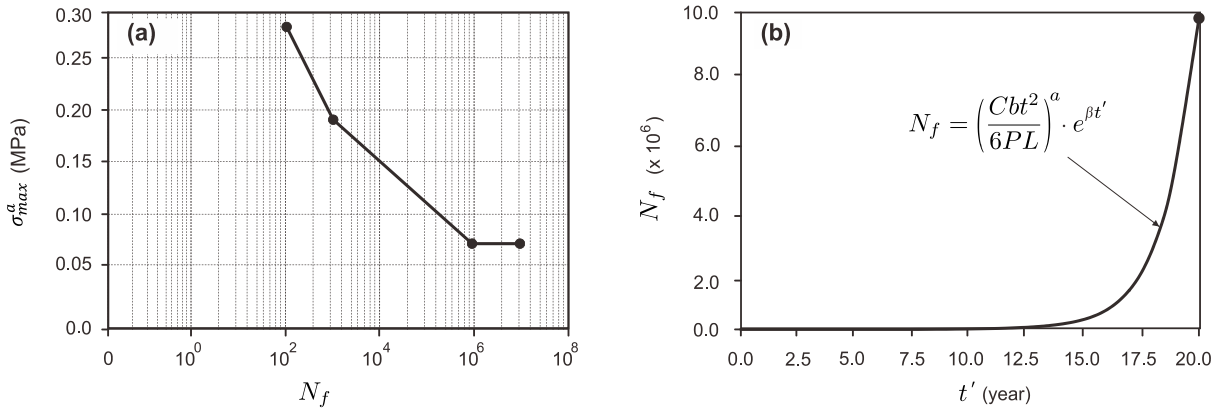

Fig. 20. Fatigue life prediction of RAC bench with racquet fibres and PTMS (Series II): (a) S-N curve, and (b) theoretical years of fatigue life.

Figs. 20a-b show, correspondingly, the S-N curve and the predicted fatigue life of the RAC bench with racquet fibres and PTMS (Series II). The S-N curve between stress (σ) and number of cycles to failure (N_f) for the RAC benches in **Fig. 20a** indicates that higher stress levels significantly reduce the fatigue life. The predicted fatigue life (**Fig. 20b**) considers time-dependent degradation factors, using Basquin's equation to consider the reduction in fatigue strength over time. The bench (without PTMS) demonstrated a theoretical fatigue life of up to 20 years under typical service conditions, highlighting the beneficial impact of incorporating racquet fibres and post-tensioning metal straps on enhancing fatigue life. This good fatigue life indicates the viability of the benches for long-term use, offering a sustainable and resilient solution for urban furniture applications.

6 Added value with glow-in-the-dark features

According to recent studies, well-lit public areas can decrease the incidence of accidents and increase the perception of safety among users [32]. Accordingly, the benches in Series II incorporated thermoplastic resin (standard road marking paint) mixed with glow-in-the-dark (GID) powder. This was done to enhance night-time visibility and aesthetic appeal to the benches. GID elements can also improve night-time visibility in dark areas.

Different amounts of GID powder (0%, 10%, 15%, 20%, 25%, and 30% by volume) were mixed with a two-part thermoplastic resin in a circular shape (10 cm diameter and 1 cm thickness) and kept in a dark box to examine the brightness over 2 h during both day and night, as shown in **Fig. 21a**. A lux meter was used to collect illuminance emitted from sunlight sources. The data were collected in August 2023 between 6.00 am and 7.30 pm at a bench built at Walailak University, Thailand. The amount of glow powder absorption significantly depends on the illuminance throughout the day. It was found that the optimum amount of GID was 25% by volume.

Fig. 21b shows that the GID in the RAC bench maintains its luminescence during both day and night (from 6.00 am to 5.00 am). Due to fluctuations in light intensity during the day, the outcome of the GID varies. It can be observed that the decay of luminescence is faster at 6.00 pm. The GID bench achieves maximum luminance when exposed to higher lux intensity (i.e. high ambient light). However, by the end of the night, the ambient luminance is much lower than at daytime, thus enabling the GID to achieve its full performance (between 6.00 pm to 6.00 am). The brightness drops back almost immediately to the intensity profile in the absence of ambient light, as shown in **Fig. 21b**. Based on the test results, it is concluded that the use of GID (i.e. 25% GID powder with thermoplastic resin) in the RAC bench offers significant value-added to urban furniture, combining innovation with practical functionality [48].

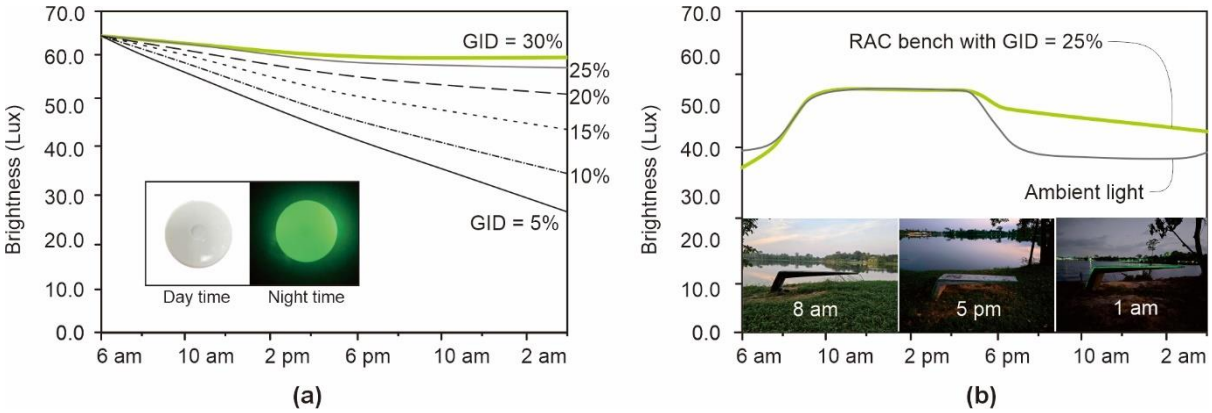

Fig. 21. Optimisation of GID with time and brightness: (a) luminance on sunny day, and (b) comparison of GID brightness with ambient light (photo taken on 30 August 2023).

Fig. 22a shows one of the urban cantilever benches at Walailak University, which has become a touristic spot within the campus. Additional benches were strategically positioned around artificial lakes within the campus, with day and night views depicted in **Figs. 22b** and **22c**. A time-lapse of the benches over a full day of service is included in Appendix C. Such benches serve now as public spaces in the streetscape where users enjoy meals, exercise and relax, thus contributing to the wellbeing of students and staff. However, future research should investigate the behaviour of the benches under other types

of loads such as high shear (e.g. [49,50]) or extreme conditions such as fire and severe environmental conditions, which are known to affect RAC more than normal concrete [51,52].

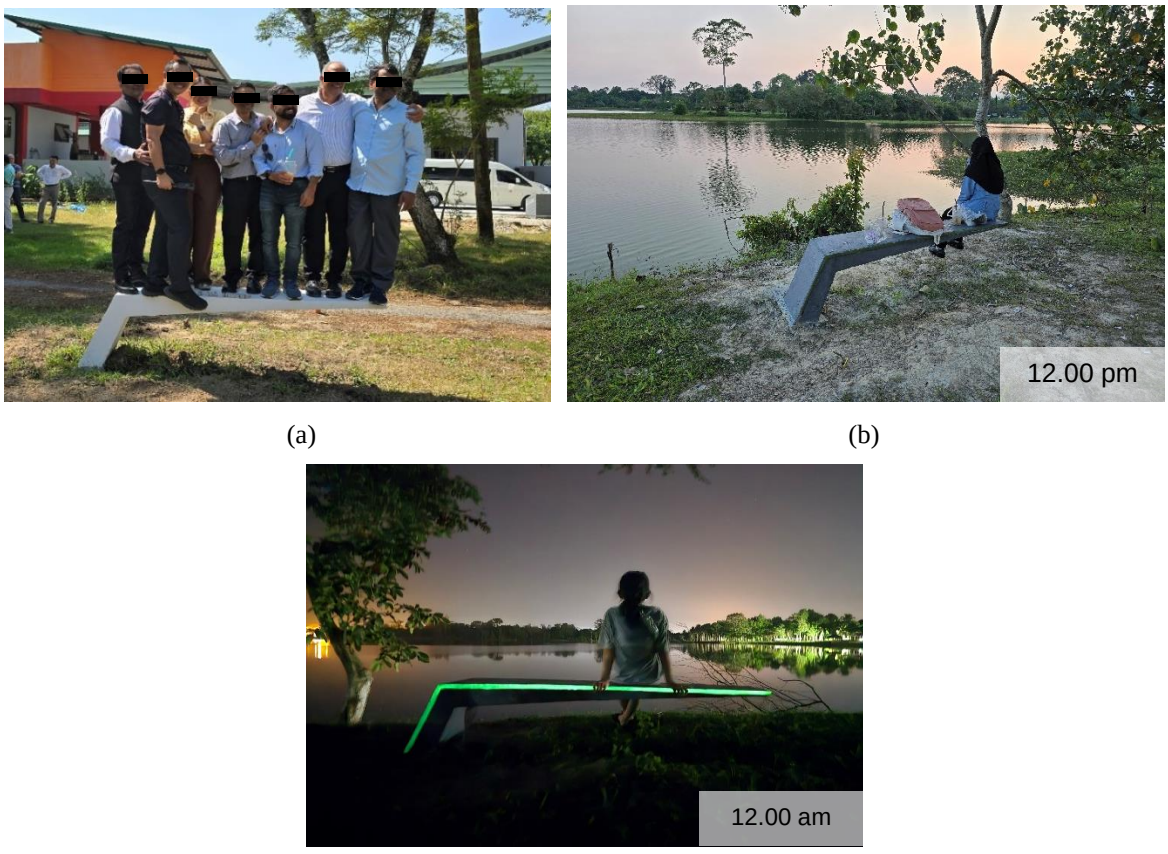

(a) (b)

(c)

Fig. 22. Typical view of benches with GID at Walailak University: (a) point for visitors, (b) view of the bench at daytime (12.00 pm), and (c) bench at night-time (12.00 am).

7 Conclusions

This study investigates the serviceability and structural behaviour of a new type of urban bench cast with recycled aggregate concrete (RAC) and waste badminton racquet fibres. Twenty-one cantilever benches were tested in two Series with different fibre volume fractions (V_f=0%, 0.5%, 1.0% and 1.5%). The RAC had 100% of the natural aggregates replaced with recycled concrete aggregate (RCA). The benches in Series II were post-tensioned in flexure using an innovative Post-Tensioned Metal Strapping (PTMS) technique using 1, 2 or 3 layers of straps. Tests were carried out to evaluate 1) static loading behaviour, 2) long-term behaviour after 365 days of sustained loading, and 3) human-induced vibrations. Finite element analyses of the RAC benches with PTMS were carried out in Abaqus® software to provide further insight into the behaviour of the benches. From the results presented in this article, the following conclusions can be drawn:

- RAC with a V_f=1.5% of racquet fibres led to a suitable balance between compressive strength and deformability. The static test results show that benches cast with RAC and a V_f=1.5% of racquet fibres had 101% higher capacity over control cantilever benches. The reduction of deflections at the tip (free end) of the benches is due to the addition of the fibres, which improve the resistance against microcracking.
- The long-term behaviour tests on benches with PTMS show that both the maximum deflections and residual deflections reduced by 24% and 56% for benches with 3 layers of PTMS when compared to counterpart benches with one layer of PTMS.

- The results obtained from human-induced vibration tests (normal walking, brisk walking and jumping) show that the maximum vibrations produced by both male and female participants met the standard values for human-induced vibrations for floor buildings.
- The incorporation of glow-in-the-dark (GID) features in the proposed cantilever benches significantly enhances night-time visibility and safety. This makes the benches highly functional as a social space, as well as visually appealing in urban settings.

Acknowledgments

The project was partially supported by the Walailak University International Mobility Fund for Research collaboration programme (Contract no. WU-CIA-00202/2024). The authors also gratefully acknowledge the India Science and Research Fellowship (ISRF) FY 2022-23 (Thailand, Malaysia and India).

Funding Statement

This research was funded by a Walailak University research grant (contract no. WU 66282).

CRediT authorship contribution statement

Narakorn Suwannachote: Investigation, Formal Analysis, Writing – Original Draft. **Thanongsak Imjai**: Conceptualization, Funding Acquisition, Supervision, Investigation, Formal Analysis, Writing – Original Draft. **Fetih Kefyalew** and **Radhika Sridhar**: Investigation. U. **Johnson Alengaram** and **Sivakumar Naganathan**: Supervision, Review & Editing. **Reyes Garcia**: Supervision, Writing – Review & Editing.

Conflicts of Interest

The authors declare that they have no conflicts of interest to report regarding the present study.

References

[1] Xiao J, Li W, Poon C. Recent studies on mechanical properties of recycled aggregate concrete in China—A review. Science China Technological Sciences 2012; 55: 1463-1480. https://doi.org/10.1007/s11431-012-4786-9.

[2] Behera M, Bhattacharyya SK, Minocha AK, Deoliya R, Maiti S. Recycled aggregate from C&D waste & its use in concrete–A breakthrough towards sustainability in construction sector: A review. Construction and Building Materials 2014; 68: 501-516. https://doi.org/10.1016/j.conbuildmat.2014.07.003.

[3] Shi C, Li Y, Zhang J, Li W, Chong L, Xie Z. Performance enhancement of recycled concrete aggregate–a review. Journal of Cleaner Production 2016; 112: 466-472. https://doi.org/10.1016/j.jclepro.2015.08.057.

[4] Neupane RP, Imjai T, Makul N, Garcia R, Kim B, Chaudhary S. Use of recycled aggregate concrete in structural members: a review focused on Southeast Asia. Journal of Asian Architecture and Building Engineering 2023; 1-24. https://doi.org/10.1080/13467581.2023.2270029.

[5] Medina C, Zhu W, Howind T, Frías M, De Rojas MS. Effect of the constituents (asphalt, clay materials, floating particles and fines) of construction and demolition waste on the properties of recycled concretes. Construction and Building Materials 2015; 79: 22-33. https://doi.org/10.1016/j.conbuildmat.2014.12.070.

[6] Oikonomou ND. Recycled concrete aggregates. Cement and Concrete Composites 2005; 27(2): 315-318. https://doi.org/10.1016/j.cemconcomp.2004.02.020.

[7] Martín-Morales M, Zamorano M, Ruiz-Moyano A, Valverde-Espinosa I. Characterization of recycled aggregates construction and demolition waste for concrete production following the Spanish Structural Concrete Code EHE-08. Construction and Building Materials 2011; 25(2): 742-748. https://doi.org/10.1016/j.conbuildmat.2010.07.012.

[8] Bandara HM, Thushanth G, Somarathna HM, Jayasinghe DH, Raman SN. Feasible techniques for valorisation of construction and demolition waste for concreting applications. International Journal of Environmental Science and Technology 2023; 20(1): 521-536. https://doi.org/10.1007/s13762-022-04015-z.

[9] Tam VW, Soomro M, Evangelista AC. A review of recycled aggregate in concrete applications (2000–2017). Construction and Building Materials 2018; 172: 272-292. https://doi.org/10.1016/j.conbuildmat.2018.03.240.

[10] Poon CS, Kou SC, Lam L. Influence of recycled aggregate on slump and bleeding of fresh concrete. Materials and Structures 2007; 40: 981-988. https://doi.org/10.1617/s11527-006-9192-y.

[11] Zhang C, Hu M, Dong L, Xiang P, Zhang Q, Wu J, Li B, Shi S. Co-benefits of urban concrete recycling on the mitigation of greenhouse gas emissions and land use change: A case in Chongqing metropolis, China. Journal of Cleaner Production 2018; 201: 481-498. https://doi.org/10.1016/j.jclepro.2018.07.238.
[12] Sánchez-Roldán Z, Martín-Morales M, Valverde-Espinosa I, Zamorano M. Technical feasibility of using recycled aggregates to produce eco-friendly urban furniture. Construction and Building Materials 2020; 250: 118890. https://doi.org/10.1016/j.conbuildmat.2020.118890.
[13] Rout A, Galpern P. Benches, fountains and trees: using mixed-methods with questionnaire and smartphone data to design urban green spaces. Urban Forestry & Urban Greening 2022; 67: 127335, https://doi.org/10.1016/j.ufug.2021.127335.
[14] Makul N, Fediuk R, Amran M, Zeyad AM, de Azevedo AR, Klyuev S, Vatin N, Karelina M. Capacity to develop recycled aggregate concrete in South East Asia. Buildings 2021; 11(6): 234. https://doi.org/10.3390/buildings11060234.
[15] Kim GB, Pilakoutas K, Waldron P. Thin FRP/GFRC structural elements. Cement and Concrete Composites 2008; 30(2): 122-137. https://doi.org/10.1016/j.cemconcomp.2007.04.011.
[16] Facconi L, Minelli F, Plizzari G. Steel fiber reinforced self-compacting concrete thin slabs–Experimental study and verification against Model Code 2010 provisions. Engineering Structures 2016; 122: 226-237. https://doi.org/10.1016/j.engstruct.2016.04.030.
[17] Suwannachote N, Imjai T, Wattanapanich C, Kefyalew F, Garcia R, Aosai P. Experimental and computer simulation studies on badminton racquet strings. Sensors 2023; 23(13): 5957. https://doi.org/10.3390/s23135957.
[18] Pešić N, Živanović S, Garcia R, Papastergiou P. Mechanical properties of concrete reinforced with recycled HDPE plastic fibres. Construction and building materials 2016; 115: 362-370. https://doi.org/10.1016/j.conbuildmat.2016.04.050.
[19] Bonopera M, Chang KC, Tullini N. Vibration of prestressed beams: Experimental and finite-element analysis of post–tensioned thin-walled box-girders. Journal of Constructional Steel Research 2023; 205: 107854. https://doi.org/10.1016/j.jcsr.2023.107854.
[20] Imjai T, Setkit M, Garcia R, Figueiredo FP. Strengthening of damaged low strength concrete beams using PTMS or NSM techniques. Case Studies in Construction Materials 2020; 13: 00403. https://doi.org/10.1016/j.cscm.2020.e00403.
[21] Helal Y, Garcia R, Pilakoutas K, Guadagnini M, Hajirasouliha I. Bond of substandard laps in RC beams retrofitted with post-tensioned metal straps. ACI Structural Journal 2016; 113(6): 1197-1208. https://doi.org/10.14359/51689021.
[22] Neupane RP, Imjai T, Garcia R, Alengaram UJ. A new constitutive model for recycled aggregate concrete cylinders actively confined with post-tensioned metal straps. Sustainable Structures 2024; 4(5): 1-22. https://doi.org/10.54113/j.sust.2024.000049.
[23] Imjai T, Garcia R, Kim B, Hansapinyo C, Sukontasukkul P. Serviceability behaviour of FRP-reinforced slatted slabs made of high-content recycled aggregate concrete Structures 2023; 51: 1071-1082. https://doi.org/10.1016/j.istruc.2023.03.075.
[24] Kefyalew F, Imjai T, Garcia R, Son NK. Fire behavior of high-contents recycled aggregate concrete composite slabs with small openings. Structural Concrete 2024. https://doi.org/10.1002/suco.202400242.
[25] Imjai T, Kefyalew F, Garcia R, Kim B, Bras A. and Sukontasukkul, P. Performance of a novel structural insulated panel in tropical climates: Experimental and numerical studies. Construction and Building Materials 2024; 421: 135568. https://doi.org/10.1016/j.conbuildmat.2024.135568.
[26] Kefyalew F, Imjai T, Garcia R, Kim B. Structural and service performance of composite slabs with high recycled aggregate concrete contents. Engineered Science 2023; 27: 2024. https://dx.doi.org/10.30919/es1021.
[27] Sridhar R, Prasad DR. Damage assessment of functionally graded reinforced concrete beams using hybrid fiber engineered cementitious composites. Structures 2019; 20: 832-847. https://doi.org/10.1016/j.istruc.2019.07.002.
[28] Sridhar R, Prasad R. Damage evaluation of functionally graded reinforced concrete beams with composite layers. Proceedings of the Institution of Civil Engineers-Structures and Buildings 2022; 175(2): 112-128. https://doi.org/10.1680/jstbu.18.00213.
[29] Kostrzewska M. Activating public space: how to promote physical activity in urban environment. In IOP Conference Series: Material Science and Engineering 2017; 5: 052074. https://iopscience.iop.org/article/10.1088/1757-899X/245/5/052074/pdf.
[30] Wen YK. Application of random vibration method to safety and damage analysis of buildings and structures. Studies in Applied Mechanics 1986; 14: 511-523. https://doi.org/10.1016/B978-0-444-42665-9.50036-0.
[31] Neupane RP, Imjai T, Garcia R. A novel post-tensioned metal strapping technique to actively confine concrete structures: A review. Innovative Infrastructure Solutions 2024. In press. https://doi.org/10.1007/s41062-024-01791-0.

[32] Wiese A, Washington T, Tao B, Weiss WJ. Assessing performance of glow-in-the-dark concrete. Transportation Research Record 2015; 2508(1): 31-38. https://doi.org/10.3141/2508-04.
[33] ASTM D3379-75. Standard test method for tensile strength and young's modulus for high-modulus single filament materials, ASTM International 1989; 100 Barr Harbor Drive, PO Box C700, West Conshohocken, PA 19428-2959, United States.
[34] ACI 211.1. Standard properties for selecting proportions for normal, heavy weight and mass concrete. American Concrete Institute 2002; Detroit: The Institute, United States.
[35] ASTM C39/C39M – 21. Standard test method for compressive strength of cylindrical concrete specimens. ASTM International 2021; 100 Barr Harbor Drive, PO Box C700, West Conshohocken, PA 19428-2959. United States.
[36] ASTM C496. Standard test method for splitting tensile strength of cylindrical concrete specimens. ASTM International 2017; 100 Barr Harbor Drive, PO Box C700, West Conshohocken, PA 19428-2959. United States.
[37] ASTM C78/C78M. Standard test method for flexural strength of concrete using simple beam with third - point loading. ASTM International 2021; 100 Barr Harbor Drive, PO Box C700, West Conshohocken, PA 19428-2959. United States.
[38] BS 6472-1. Guide to evaluation of human exposure to vibration in buildings – vibration sources other than blasting. British Standards 2008; British standard institutions - Publisher.
[39] ISO 2631-2. Mechanical vibration and shock - Evaluation of human exposure to whole body vibration (1 Hz to 80 Hz). International Organization for Standardization 2003; ISO 2003. Published in Switzerland.
[40] ISO 2631-1. Mechanical vibration and shock- evaluation of human exposure to whole-body vibration -part 2: Vibration in buildings (1 Hz to 80 Hz). International Organization for Standardization 1997; ISO 1997. Published in Switzerland.
[41] Imjai T, Aosai P, Garcia R, Raman SN, Chaudhary S. Deflections of high-content recycled aggregate concrete beams reinforced with GFRP bars and steel fibres. Engineering Structures 2024; 312: 118247. https://doi.org/10.1016/j.engstruct.2024.118247.
[42] Genikomsou AS, Polak MA. Damaged plasticity modelling of concrete in finite element analysis of reinforced concrete slabs. In 9th International Conference on Fracture Mechanics of Concrete and Concrete Structures University of California 2016; 22-25. http://doi.org/10.21012/FC9.006.
[43] Al-Zuhairi AH, Al-Ahmed AH, Abdulhameed AA, Hanoon AN. Calibration of a new concrete damage plasticity theoretical model based on experimental parameters. Civil Engineering Journal 2022; 8(2): 225-237. http://dx.doi.org/10.28991/CEJ-2022-08-02-03.
[44] Birtel VA, Mark P. Parameterised finite element modelling of RC beam shear failure. In: ABAQUS users' conference 2006; 23(14).
[45] Krätzig WB, Pölling R. An elasto-plastic damage model for reinforced concrete with minimum number of material parameters. Computers and Structures 2004; 82(15-16): 1201-1215. https://doi.org/10.1016/j.compstruc.2004.03.002.
[46] Foote RM, Mai YW, Cotterell B. Crack growth resistance curves in strain-softening materials. Journal of the Mechanics and Physics of Solids 1986; 34(6): 593-607. https://doi.org/10.1016/0022-5096(86)90039-6.
[47] Lee DH, Hwang JH, Ju H, Kim KS, Kuchma DA. Nonlinear finite element analysis of steel fiber-reinforced concrete members using direct tension force transfer model. Finite Elements in Analysis and Design 2012; 50: 266-286. https://doi.org/10.1016/j.finel.2011.10.004.
[48] Saleem M, Blaisi NI. Development, testing, and environmental impact assessment of glow-in-the-dark concrete. Structural Concrete 2019; 20(5): 1792-1803. https://doi.org/10.1002/suco.201800221.
[49] Imjai T, Kefyalew F, Aosai P, Garcia R, Kim B, Abdalla HM, Raman SN. A new equation to predict the shear strength of recycled aggregate concrete Z push-off specimens. Cement and Concrete Research 2023; 169: 107181. https://doi.org/10.1016/j.cemconres.2023.107181.
[50] Leelatanon S, Imjai T, Setkit M, Garcia R, Kim B. Punching shear capacity of recycled aggregate concrete slabs. Buildings 2022; 12(10): 1584. https://doi.org/10.3390/buildings12101584.
[51] Kefyalew F, Imjai T, Garcia R, Khanh Son N, Chaudhary S. Performance of recycled aggregate concrete composite metal decks under elevated temperatures: a comprehensive review. Journal of Asian Architecture and Building Engineering 2024; 1-23. https://doi.org/10.1080/13467581.2024.2309347.
[52] Wattanapanich C, Imjai T, Sridhar R, Garcia R, Thomas BS. Optimizing recycled aggregate concrete for severe conditions through machine learning techniques: A review. Engineered Science 2024; 31: 1191. http://dx.doi.org/10.30919/es1191.

Appendix A.

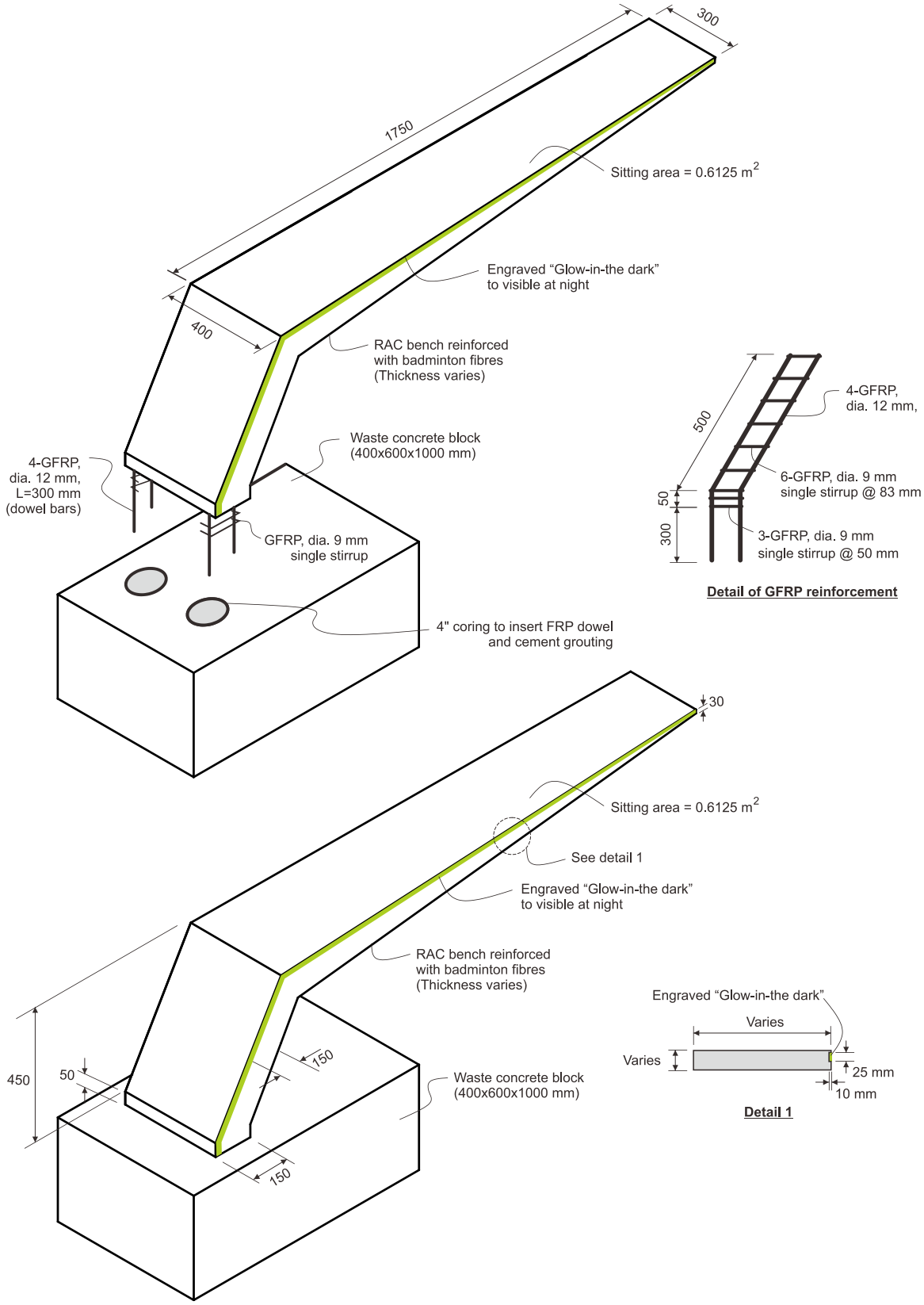

Fig. A-1. Bench geometry, reinforcement details and construction of RAC cantilever bench.

Appendix B. Fatigue life prediction of recycled aggregate concrete bench

From the short-term tests, the load applied on the bench is 27,000 N and the deformation is 2.3 mm. The bench has a length L=1700 mm (measured at the neutral axis position).

Cross-sectional dimensions:

- Width b=400 mm
- Thickness t_b=50 mm at the base
- Cantilever length (L): 1700 mm
- Height (H): 450 mm
- Thickness at tip (t*): 25 mm
- Concrete base dimensions: 1000 mm (length) ×400 mm (width) ×600 mm (height)

First, calculate the moment of inertia (I) for a rectangular cross-section using Equation B.1.

$$I = \frac{bt_b^3}{12} = \frac{400 * 50^3}{12} = \frac{400 * 125000}{12} = 4.1667 * 10^3\ mm^4 \quad \text{(B. 1)}$$

Calculate the maximum bending stress (σ_{max}) at the base, as shown in Equation B.2.

$$\sigma_{max} = \frac{M_{max} * y}{I} \quad \text{(B. 2)}$$

where $M_{max} = P * L = 27000 * 1700 = 4.59 * 10^7$ Nmm, and $y = \frac{t_b}{2} = \frac{50}{2} = 25$ mm

$$\sigma_{max} = \frac{4.59 * 10^7\ \text{Nmm} * 25\ \text{mm}}{4.1667 * 10^3\ \text{mm}^4} = 275.6\ \text{MPa}$$

To estimate the number of cycles at failure (N_f) at different loads considering the static load test results, a linear relationship is considered between load and deflection to estimate equivalent stresses and cycles at failure for loads 10 kN, 20 kN, and 27 kN at corresponding deformations 0.85 mm, 1.7 mm, and 2.3 mm. The corresponding stress calculated by bending moment:

$$M_{max1} = 10 * 10^3 * 1700 = 1.7 * 10^7\ \text{Nmm}$$
$$\sigma_{max1} = \frac{1.7 * 10^7 * 25}{4.1667 * 10^6} = 102\ \text{MPa}$$
$$M_{max2} = 20 * 10^3 * 1700 = 3.4 * 10^7\ \text{Nmm}$$
$$\sigma_{max2} = \frac{3.4 * 10^7 * 25}{4.1667 * 10^6} = 204\ \text{MPa}$$
$$M_{max2} = 27 * 10^3 * 1700 = 4.59 * 10^7\ \text{Nmm}$$
$$\sigma_{max2} = \frac{3.4 * 10^7 * 25}{4.1667 * 10^6} = 275.6\ \text{MPa}$$

To Fit Basquin's Law, it is possible to consider the fatigue test data recorded at each load 10^6, 10^5 and 10^4 cycles respectively. Using this data point of stress and cycles at failure (shown in **Table B.1**), fatigue test data have been converted to logarithmic scale (see **Table B.2**).

Table B.1. Fatigue test data recorded at different failure cycle

Stress σ (MPa)	Cycles to failure (N_f)
102	10^6
204	10^5
275.6	10^4

Table B.2. Transfer to logarithmic scale

log (σ)	log (Nf)
log (102)	(106)
log (204)	(105)
log (275.6)	(104)
log (σ)	log (Nf)

Consider Fit Basquin's Law

The data points of stress can be calculated from Equation B.3:

$$\text{Log}(\sigma) = \log(C) - a*\log(N_f) \quad \text{(B.3)}$$

Given the data points and Log-Log Data for Basquin's Law:

$\sigma_1 = 102\ Mpa, \sigma_2 = 204\ Mpa, \sigma_3 = 275.6\ Mpa$ and the corresponding fatigue life $N_{f1} = 10^6$, $N_{f2} = 10^5$, and $N_{f3} = 10^4$.

Accordingly, the corresponding logarithmic function becomes:

$log\ log\ (\sigma_1) = log\ log\ (102) = 2.0086$

$log\ log\ (\sigma_2) = log\ log\ (204) = 2.3096$

$log\ log\ (\sigma_3) = log\ log\ (275.6) = 2.4409$

$log\ (N_{f1}) = \log(10^6) = 6$

$log\ (N_{f2}) = \log(10^5) = 5$

$log\ (N_{f3}) = \log(10^4) = 4$

Use the points ($log\ (N_f)$, $log\ log\ (\sigma)$) to perform linear regression:

($log\ (N_f)$, $log\ log\ (\sigma)$): $(6, 2.0086), (5, 2.3096), and\ (4, 2.4409)$

The linear regression equation is shown in Equation B.4:

$$log\ log\ (\sigma) = log\ log\ (C) - a*log\ log\ (N_f) \quad \text{(B.4)}$$

- Calculation of slope and intercept using the least squares method (Linear Regression calculation).

The general formula for the slope *m* and intercept *b* in a linear regression *y*=m*x*+*b* is given in Equations B.5 and B.6.

$$m = \frac{n(\sum xy) - (\sum x)(\sum y)}{n((\sum x^2) - (\sum x)^2)} \quad \text{(B.5)}$$

$$b = \frac{(\sum y)(\sum x^2) - (\sum x)(\sum xy)}{n(\sum x^2) - (\sum x)^2)} \quad \text{(B.6)}$$

where: $x = log\ log\ (N_f)$, y = $log\ log\ (\sigma)$, $n =$ number of data points $= 3$

Calculating the summation:

$$\sum x = 6 + 5 + 5 = 15,$$

$$\sum y = 2.008 + 2.3096 + 2.4409 = 6.7591$$

$$\sum x = 6 + 5 + 4 = 15,$$

$$\sum x^2 = 6^2 + 5^2 + 4^2 = 77$$

$$\sum y^2 = 2.008^2 + 2.3096^2 + 2.4409^2 = 77$$

$$\sum xy = 2.008 * 6 + 2.3096 * 5 + 2.4409 * 4 = 33.0786$$

Using these sums, the slope *m* and intercept *b* are:

$$m = \frac{3(33.0786) - (15)(6.7591)}{3((77) - (15)^2)} = \frac{99.2358 - 101.3865}{231 - 225} = \frac{-2.1507}{6} = -0.3585$$

$$\text{b} = \frac{(6.7591)(77) - (15)(33.0786)}{3((77) - (15)^2)} = \frac{520.6547 - 496.179}{231 - 225} = \frac{24.4757}{6} = 4.0793$$

Therefore, $a = -m = 0.3585$

$\log(C) = b = 4.0793$

$c = 10^{4.0793} = 12000$

The degradation can be calculated from Equation B.7:

$$log\ log\left(\sigma_f(t)\right) = log\ log\left(\sigma_{f0}\right) - \beta t' \quad \text{(B.7)}$$

where $\sigma_{f0} = \sigma_1 = 102$ MPa, and at a sustained load test recorded $\sigma_f(t) = 50$ MPa, over one year (365 days)

$$50MPa = 102MPa - \beta(365 \text{ days})$$

$$\frac{50}{102} = e^{-\beta * 365}$$

$$ln\left(\frac{50}{102}\right) = -\beta * 365$$

$$\beta = -\frac{lnln\ (0.4902)}{365} = \frac{0.7123}{365} = 0.00195\ \text{day}^{-1}$$

Appendix C. Timelapse of RAC bench with glow-in-the-dark features: https://youtu.be/pSdIi0jj65w